Chemical Science

ROYAL SOCIETY OF CHEMISTRY

EDGE ARTICLE

View Article Online
View Journal | View Issue

Cite this: *Chem. Sci.*, 2021, **12**, 13216

All publication charges for this article have been paid for by the Royal Society of Chemistry

Received 10th July 2021
Accepted 10th September 2021

DOI: 10.1039/d1sc03756k

rsc.li/chemical-science

Supramolecular photocatalysts fixed on the inside of the polypyrrole layer in dye sensitized molecular photocathodes: application to photocatalytic CO_2 reduction coupled with water oxidation†

Fazalurahman Kuttassery, ‡[a] Hiromu Kumagai, [b] Ryutaro Kamata,[a] Yusuke Ebato,[a] Masanobu Higashi, [c] Hajime Suzuki, [d] Ryu Abe [d] and Osamu Ishitani *[a]

The development of systems for photocatalytic CO_2 reduction with water as a reductant and solar light as an energy source is one of the most important milestones on the way to artificial photosynthesis. Although such reduction can be performed using dye-sensitized molecular photocathodes comprising metal complexes as redox photosensitizers and catalyst units fixed on a p-type semiconductor electrode, the performance of the corresponding photoelectrochemical cells remains low, *e.g.*, their highest incident photon-to-current conversion efficiency (IPCE) equals 1.2%. Herein, we report a novel dye-sensitized molecular photocathode for photocatalytic CO_2 reduction in water featuring a polypyrrole layer, $[Ru(diimine)_3]^{2+}$ as a redox photosensitizer unit, and $Ru(diimine)(CO)_2Cl_2$ as the catalyst unit and reveal that the incorporation of the polypyrrole network significantly improves reactivity and durability relative to those of previously reported dye-sensitized molecular photocathodes. The irradiation of the novel photocathode with visible light under low applied bias stably induces the photocatalytic reduction of CO_2 to CO and HCOOH with high faradaic efficiency and selectivity (even in aqueous solution), and the highest IPCE is determined as 4.7%. The novel photocathode is coupled with n-type semiconductor photoanodes (CoO_x/$BiVO_4$ and RhO_x/TaON) to construct full cells that photocatalytically reduce CO_2 using water as the reductant upon visible light irradiation as the only energy input at zero bias. The artificial Z-scheme photoelectrochemical cell with the dye-sensitized molecular photocathode achieves the highest energy conversion efficiency of 8.3×10^{-2}% under the irradiation of both electrodes with visible light, while a solar to chemical conversion efficiency of 4.2×10^{-2}% is achieved for a tandem-type cell using a solar light simulator (AM 1.5, 100 mW cm^{-2}).

Introduction

The reduction of CO_2 to useful carbon resources using sunlight as the energy source and water as the electron donor is expected to provide a sustainable solution to the energy and environmental problems currently facing our society.[1,2] In this regard, photocatalytic CO_2 reduction systems with transition metal complexes acting as (i) redox photosensitizers that absorb visible light to initiate electron transfer and (ii) catalysts that accept electrons from redox photosensitizers to reduce CO_2 have drawn much attention, as these complexes exhibit tunable visible light absorption and redox properties as well as high CO_2 reduction selectivity.[3,4] For example, a mixed system comprising $[Ru(bpy)_3]^{2+}$ (bpy = 2,2′-bipyridine) as the redox photosensitizer and $[Ru(X_2bpy)(CO)_2Cl_2]$ as the catalyst efficiently and selectively catalyses the photoreduction of CO_2 in the presence of sacrificial electron donors such as 1-benzyl-1,4-dihydronicotinamide to give CO and HCOOH, the ratio of

[a]*Department of Chemistry, Tokyo Institute of Technology, 2-12-1-NE-1, O-okayama, Meguro-ku, Tokyo 152-8550, Japan. E-mail: ishitani@chem.titech.ac.jp*

[b]*Institute of Multidisciplinary Research for Advanced Materials, Tohoku University, 2-1-1, Katahira, Aoba-ku, Sendai, Miyagi 980-8577, Japan*

[c]*The OCU Advanced Research Institute for Natural Science and Technology, Osaka City University, 3-3-138 Sugimoto, Sumiyoshi-ku, Osaka City, Osaka 558-8585, Japan*

[d]*Department of Energy and Hydrocarbon Chemistry, Graduate School of Engineering, Kyoto University, Katsura, Nishikyo-ku, Kyoto 615-8510, Japan*

† Electronic supplementary information (ESI) available: Synthetic strategy and ^{1}H-NMR spectra of metal complexes synthesized (SI-I), additional electrochemical, characterization, photoelectrochemical CO_2 reduction and single cell artificial Z-scheme data (Fig. S1–S10). Quantitative estimation of Ru(II) by ICP-MS analysis of photocathodes (Tables S1–S4), Summary of photoelectrochemical CO_2 reduction under controlled experimental conditions (Table S5). See DOI: 10.1039/d1sc03756k

‡ Present address: Department of Chemistry, University of Calicut, Malappuram, Kerala 673635, India.

which can be controlled by changing the reaction conditions such as solution pH and bpy substituents (X).[5–7] Despite the abundance of photocatalytic systems that comprise only metal complexes and can efficiently promote the photoreduction of CO_2 in the presence of sacrificial electron donors, these systems cannot use water as an electron donor owing to their relatively low oxidation power and the difficulty of the four-electron oxidation of two water molecules. However, in order to be practical, photocatalytic CO_2 utilization systems should inevitably employ water as an electron donor owing to its low cost and abundance.[8]

Hybrid systems that comprise metal complexes as (photo) catalysts and semiconductor materials and feature excited states with oxidation powers sufficient to oxidize water to O_2 and/or H_2O_2 have been actively investigated to mitigate the above problem.[9–11] Most of such hybrid systems are photoelectrochemical cells featuring a photocathode for CO_2 reduction and a photoanode for water oxidation, with the sequential excitation of these photoelectrodes endowing them with strong reduction and oxidation powers.[8] Such photoelectrochemical cells, also known as artificial Z-scheme cells, can be broadly classified into two groups, both of which feature n-type semiconductor photoanodes (*e.g.*, CoO_x-deposited $BiVO_4$ (ref. 12) and reduced $SrTiO_3$ (ref. 13)) for water oxidation. In the first group, the photocathode comprises a metal complex that is deposited on a visible-light-responsive semiconductor material and acts a CO_2 reduction catalyst but does not absorb light, *i.e.*, light is absorbed only by the semiconductor electrode (Scheme 1a).[13–15] The systems of the second group feature dye-sensitized molecular photocathodes consisting of a p-type semiconductor and a supramolecular photocatalyst with redox photosensitizer and catalyst units connected to each other (Scheme 1b).[10–12] The redox photosensitizer unit absorbs light and then transfers an electron from the valence band of the p-type semiconductor to the catalyst unit, which reduces CO_2. The hole produced in the valence band of the p-type semiconductor is filled with an electron from the n-type semiconductor photoanode, which photochemically draws up electrons from water. Therefore, in these systems, the p-type semiconductor does not absorb light, which is their largest difference from the systems of the first group. As the two systems differ in their requirements for metal complexes and semiconductor materials, one expects a broad range of suitable complexes and materials as well as construction methods. Despite the availability of photoelectrochemical cells that promote CO_2 photoreduction using water as an electron donor and visible light as an energy source, their performance metrics, especially the efficiency of light energy to chemical energy conversion, are still low.

Although the photoelectrochemical systems of the second group are very rare examples of the use of molecular photocatalysts for CO_2 reduction coupled with water oxidation,[10–12] these systems can potentially employ various redox photosensitizers with strong absorption in the visible region, which is advantageous for visible-light-driven photocathode construction. The dye-sensitized molecular photocathodes[16,17] initially reported by Meyers *et al.*[18,19] and our groups[9–11] featured metal complex-based photocatalysts with anchoring groups such as

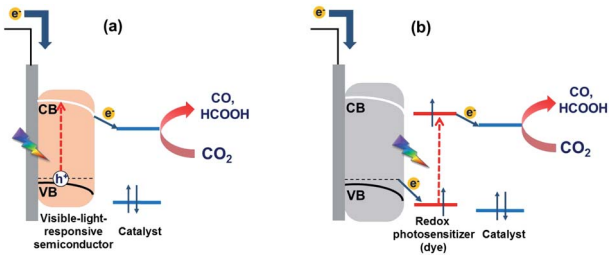

Scheme 1 Two types of photocathodes for photoelectrochemical CO_2 reduction. (a) Systems comprising a p-type semiconductor as the light absorbing unit and a metal complex as the catalyst. (b) Systems with dye-sensitized molecular photocathodes comprising a redox photosensitizer as the light absorbing unit, a metal complex as the catalyst, and a p-type semiconductor as the electron relay. VB = valence band, CB = conduction band.

–COOH and $–PO_3H_2$ adsorbed on the electrode surface. In these systems, the photosensitizer units are only monomolecularly adsorbed on the electrode, and the visible light absorption abilities of such dye-sensitized molecular photocathodes are therefore very low. In addition, the rapid detachment of the metal complex-based photocatalysts from the electrode due to weak immobilization *via* anchoring groups results in low photocathode durability.[20–23] As the absorption ability of a single photosensitizer molecule is not high, the number of photosensitizer units on the p-type semiconductor electrode should be increased to elevate the corresponding light absorption ability.

The methods of overcoming these bottlenecks can be broadly classified into two main types. On the one hand, one can introduce a protective metal oxide layer by atomic layer deposition to increase the durability of the dye-sensitized molecular photocathode by suppressing the detachment of metal complexes with anchoring groups.[24–26] However, this approach does not increase the visible light absorption of the photocathode. Methods of the second type rely on the introduction of a polymer layer, *e.g.*, Meyers'[19] and our[12,27] groups employed the reductive electropolymerization of vinyl groups in the diimine ligands of metal complexes to afford a polymer layer that contained both the photosensitizer and catalyst units on the semiconductor electrode and, compared to the photoelectrode with only the anchoring groups described above, more strongly absorbed visible light owing to the accumulation of photosensitizer units.[19,27–32] The reductive electropolymerization of molecular complexes on the dye-sensitized

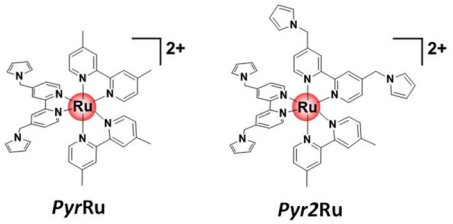

Scheme 2 Molecular structures of Ru sensitizers (*Pyr*Ru and *Pyr*2Ru) containing the *Pyr*bpy ligand(s).

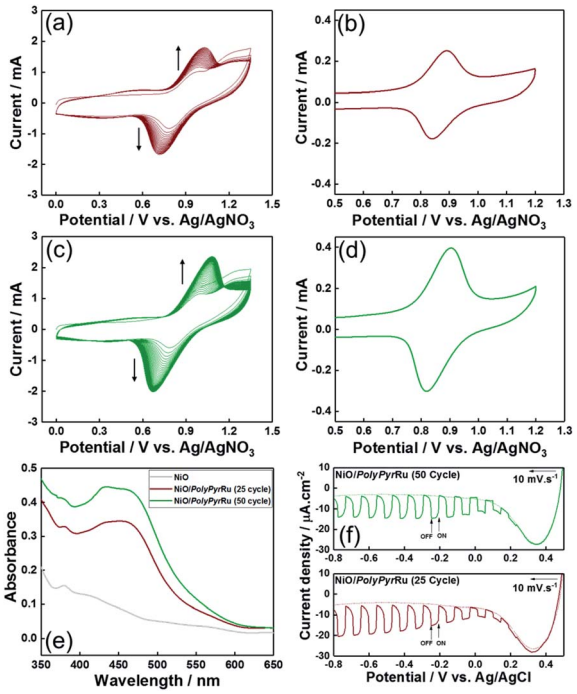

Fig. 1 Cyclic voltammograms recorded during the oxidative electropolymerization of *Pyr*Ru on NiO (electrode area = 2.5 cm^2) in Ar-saturated MeCN containing *Pyr*Ru (0.5 mM) and Et_4NBF_4 (0.1 M): (a) 25 and (c) 50 cycles between 0 and +1.35 V *vs.* $Ag/AgNO_3$ at 100 mV s^{-1}. Cyclic voltammograms of NiO/*PolyPyr*Ru as the working electrode recorded in MeCN containing 0.1 M Et_4NBF_4 as the electrolyte (counter electrode = Pt coil, reference electrode = $Ag/AgNO_3$) at 10 mV s^{-1}: (b) 25 and (d) 50 cycles. (e) DR spectra of NiO/*PolyPyr*Ru and bare NiO electrodes. (f) Visible light responses of the *I*–*V* plots of NiO/*PolyPyr*Ru working electrodes (area = 2.5 cm^2) in CO_2-purged 50 mM $NaHCO_3$ (electrolyte) recorded using a Xe lamp with a Y-48 cutoff filter (λ = 460–650 nm), a Pt coil counter electrode and a Ag/AgCl reference electrode.

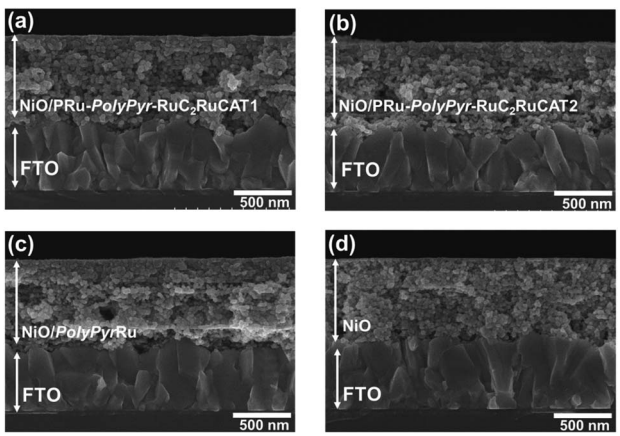

Fig. 2 SEM (side view) images of (a) NiO-PRu-*PolyPyr*-RuC_2RuCAT1 after 25 cycles, (b) NiO/PRu-*PolyPyr*-RuC_2RuCAT2, (c) NiO/*PolyPyr*Ru, and (d) NiO on FTO.

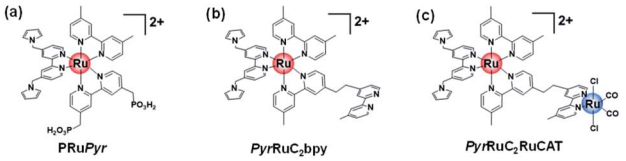

Scheme 3 Molecular structures of (a) PRu*Pyr*, (b) *Pyr*RuC_2bpy, and (c) *Pyr*RuC_2RuCAT.

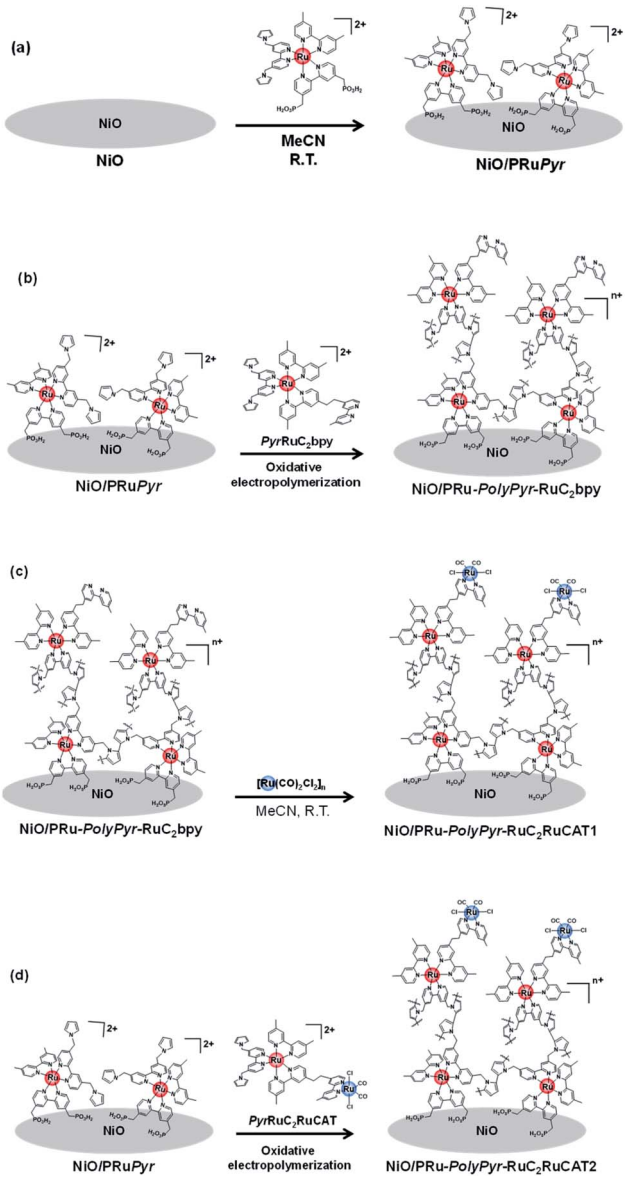

Scheme 4 Preparation of (a) NiO/PRu*Pyr* (step 1), (b) NiO/PRu-*Poly-Pyr*-RuC_2bpy (step 2), and (c) NiO/PRu-*PolyPyr*-RuC_2RuCAT1 (step 3) electrodes of a three step method of photocathode fabrication and (d) fabrication of NiO/PRu-*PolyPyr*-RuC_2RuCAT2 electrode by a two-step method (step 2).

molecular photocathode also drastically suppressed the desorption of metal complexes from the electrode and enhanced the durability of photocatalysts for CO_2 reduction.[19,27]

However, the dye-sensitized molecular photocathodes prepared *via* the reductive polymerization of vinyl groups required a relatively negative applied potential to achieve maximal

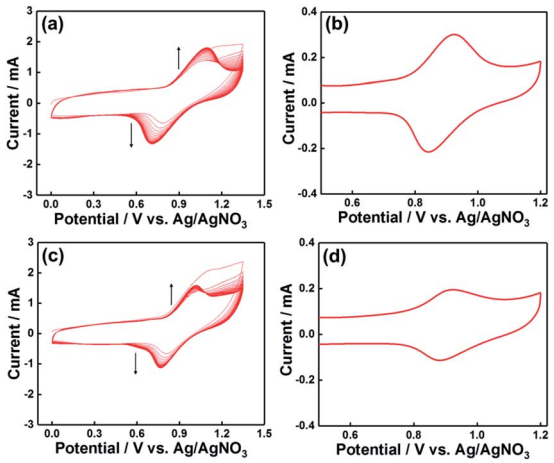

Fig. 3 Cyclic voltammograms recorded during the electropolymerization of (a) *Pyr*RuC$_2$bpy and (c) *Pyr*RuC$_2$RuCAT on NiO/PRu*Pyr* (area = 2.5 cm^2) in Ar-saturated MeCN containing the corresponding complex (0.5 mM) and Et_4NBF_4 (0.1 M) as an electrolyte. The applied potential was repeatedly cycled (25 times) between 0 and +1.35 V *vs.* Ag/AgNO$_3$ at 100 mV s^{-1}. Cyclic voltammograms of (b) NiO/PRu-*PolyPyr*-RuC$_2$RuCAT1 and (d) NiO/PRu-*PolyPyr*-RuC$_2$-RuCAT2 electrodes recorded in Ar-purged MeCN containing 0.1 M Et_4NBF_4 using a Ag/AgNO$_3$ reference electrode and a Pt counter electrode (scan rate = 10 mV s^{-1}).

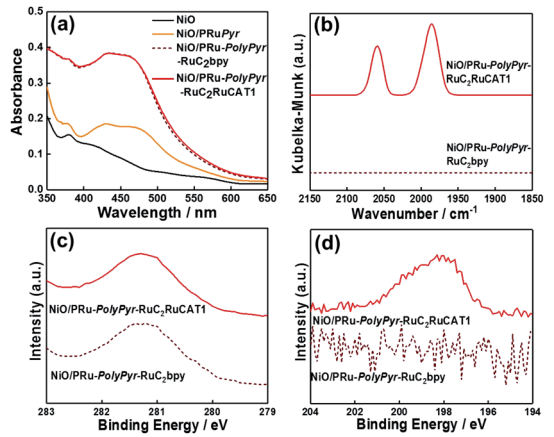

Fig. 4 (a) UV-vis (DR) absorption spectra of NiO/PRu-*PolyPyr*-RuC$_2$-RuCAT1 prepared by the three-step method (red), NiO (black), and samples obtained after process 1 (NiO/PRu*Pyr*, orange) and process 2 (NiO/PRu-*PolyPyr*-RuC$_2$bpy, dotted brown). (b) FT-IR (DR) spectra of NiO/PRu-*PolyPyr*-RuC$_2$RuCAT1 (red) and NiO/PRu-*PolyPyr*-RuC$_2$bpy (dotted brown) recorded at a scan rate of 2 cm^{-1} s^{-1}. (c) Ru 3d and (d) Cl 2p X-ray photoelectron spectra of NiO/PRu-*PolyPyr*-RuC$_2$RuCAT1 (red) and NiO/PRu-*PolyPyr*-RuC$_2$bpy (dotted brown).

photocurrent, and the photocurrent density remained low, probably because of the low conductivity of the saturated hydrocarbon chains formed by vinyl group polymerization. As a result, the incident photon-to-current conversion efficiencies (IPCEs) were 1.2% or less.[12] A photoelectrochemical cell comprising the dye-sensitized molecular photocathode fabricated by the reductive polymerization of vinyl groups and a CoO_x/$BiVO_4$ photoanode was reported as the most robust

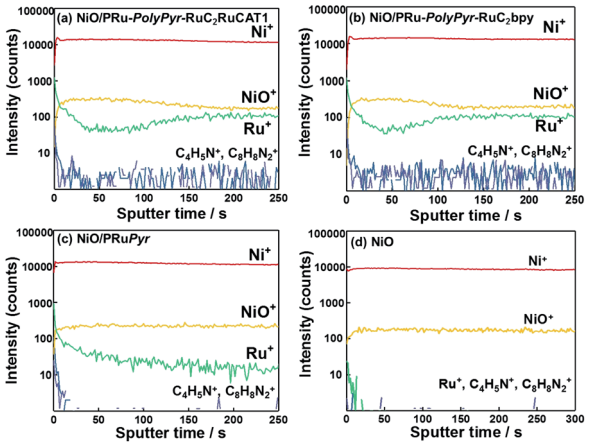

Fig. 5 TOF-SIMS spectra of (a) NiO/PRu-*PolyPyr*-RuC$_2$RuCAT1, (b) NiO/PRu-*PolyPyr*-RuC$_2$bpy, (c) NiO/PRu*Pyr*, and (d) NiO electrodes.

photocatalytic system for CO_2 reduction with water without any external bias, with the photoenergy conversion efficiency (ECE) reaching 1.7 × 10^{-2}%.[12]

The replacement of saturated hydrocarbon chains in photocathodes with conductive polymers is a promising way of reducing polymer layer resistance and increasing the efficiency of the dye-sensitized molecular photocathode. In this regard, pyrrole and its derivatives have attracted much attention owing to their high oxidative polymerization ability, relatively mild polymerization conditions, synthetic versatility, and the high conductivity of the produced polypyrrole films.[28,29,33–35] Functional polypyrrole films containing metal complex units have been reported for various applications, *e.g.*, catalytic reactions, sensors, and drug delivery.[28,29,33–41] Deronzier *et al.* reported that a system with a polypyrrole layer containing a Re(I) complex catalyst on Pt electrodes showed higher durability for electrocatalytic CO_2 reduction than the system with the corresponding mononuclear Re(I) complex in solution.[33,36,42] Morikawa *et al.* deposited a polypyrrole layer containing a Ru(II) complex catalyst onto a p-type semiconductor photoelectrode, *i.e.*, used a method of the first type according to the abovementioned classification.[14,43–46] However, the construction of dye-sensitized molecular photocathodes with conducting polypyrrole for combining redox photosensitizer molecules and a p-type semiconductor electrode has not been reported so far.

Herein, we prepare new dye-sensitized molecular photocathodes *via* the formation of polypyrrole films containing both the photosensitizer and catalytic metal complexes on NiO electrodes and systematically investigate the molecular design of metal complex monomers with pyrrole groups as well as oxidative polymerization methods to develop the most efficient dye-sensitized molecular photocathode for CO_2 reduction (maximum IPCE = 4.7%). The developed photocathode is combined with two n-type semiconductor photoanodes (CoO_x/$BiVO_4$ and RhO_x/TaON) for water oxidation to develop systems for the photoelectrocatalytic reduction of CO_2 with water using visible light as the only energy input, and the maximum ECE is determined as 8.3 × 10^{-2}%.

Table 1 Amounts of the adsorbed Ru(II) complexes in the electrodes and ratios between photosensitizers and catalysts

Sample	$n_{Rutotal}$[a] (nmol)	n_{RuPS}[b] (nmol)	n_{RuCAT}[c] (nmol)	$n_{RuPS} : n_{RuCAT}$
NiO/PRu*Pyr*	15.5	15.5	0	—
NiO/PRu-*PolyPyr*-RuC$_2$bpy	75.4	75.4	0	—
NiO/PRu-*PolyPyr*-RuC$_2$RuCAT1	100.3	75.4	24.9[c]	3 : 1
NiO/PRu-*PolyPyr*-RuC$_2$RuCAT2	40.7	28.1	12.1[c]	2.3 : 1

[a] Total amount in the electrode, which was estimated by using ICP-MS analysis. [b] Amount of the photosensitizers. [c] Amount of the catalysts.

Results and discussion

Optimization of redox photosensitizer layer on electrodes

Initially, we attempted to develop suitable polymerization methods for Ru(II) complexes with pyrrole groups on the NiO electrode, for which two types of Ru(II) trisdiimine complexes containing one or two diimine ligand(s) with two pyrrole groups, that is, 4,4′-bis((1*H*-pyrrol-1-yl)methyl)-2,2′-bipyridine ligand (*Pyr*bpy), were synthesized (*Pyr*Ru and *Pyr*2Ru in Scheme 2). The cyclic voltammograms of these complexes recorded under Ar in acetonitrile (MeCN) containing 0.1 M Et_4NBF_4 are shown in Fig. S1a and S1c,† respectively. In the case of *Pyr*Ru, one reversible and one irreversible oxidation wave were observed at $E^{ox}_{1/2}$ = 0.86 V and E^{ox}_{p} = 1.19 V *vs.* Ag/AgNO$_3$, respectively; the former was attributed to the one-electron oxidation of the central Ru(II) to Ru(III), as that of $[Ru(dmb)_3]^{2+}$ (dmb = 4,4′-dimethyl-2,2′-bipyridine) is observed at $E^{ox}_{1/2}$ = 0.77 V,[47] and the latter was attributed to the oxidation of pyrrole groups. On the other hand, the cyclic voltammogram of *Pyr*2Ru featured only one broad large oxidation wave at E^{ox}_{p} = 1.00 V, which was attributed to the combination of Ru(II) → Ru(III) oxidation and pyrrole group oxidation. These results suggest that the oxidative polymerization of the pyrrole groups of *Pyr*2Ru and *Pyr*Ru may proceed at a potential more positive than ~1 V. Both cyclic voltammograms recorded at negative potentials featured three reversible reduction waves attributable to the stepwise one-electron reduction of the diimine ligands of the Ru complexes as reported earlier (Fig. S1b and S1d†).[47]

A NiO nanoparticle-modified transparent fluorine-doped tin oxide (FTO) electrode was prepared by the previously reported squeeze method[9,10] and used as the working electrode for the oxidative electropolymerization (induced by 25 or 50 potential sweeps between E = 0 and +1.35 V *vs.* Ag/AgNO$_3$) of Ru(II) complexes with pyrrole groups. Fig. 1a shows the *I*–*V* curves of *Pyr*Ru recorded for 25 sequential potential sweeps, revealing that the current increased with increasing sweep number. The cyclic voltammogram of the electrode after 25 sweeps (Fig. 1b)

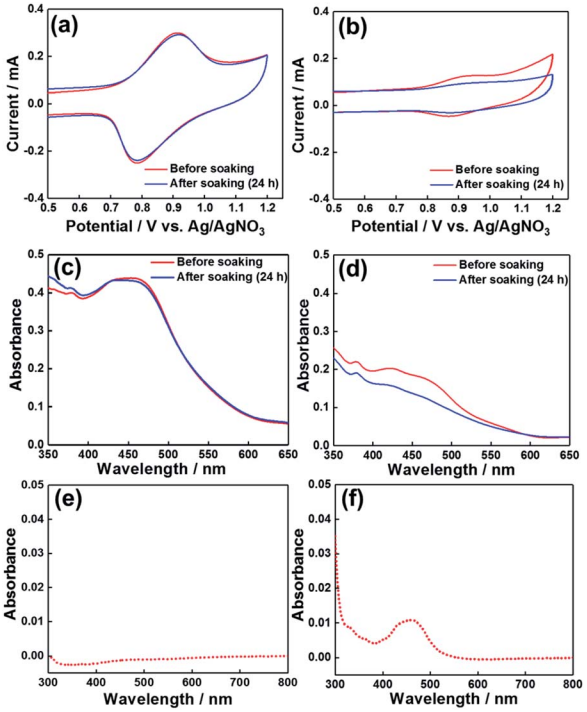

Fig. 6 Stability of photocathodes against 24 h soaking in 50 mM aqueous $NaHCO_3$ in the dark. Cyclic voltammograms of (a) NiO/PRu-*PolyPyr*-RuC$_2$RuCAT1 and (b) NiO/PRu*Pyr* before and after soaking. UV-vis (DR) absorption spectra of (c) NiO/PRu-*PolyPyr*-RuC$_2$RuCAT1 and (d) NiO/PRu*Pyr* before and after soaking. UV-vis absorption spectra of soaking solutions obtained for (e) NiO/PRu-*PolyPyr*-RuC$_2$RuCAT1 and (f) NiO/PRu*Pyr*.

Table 2 Density of the adsorbed Ru complexes on the electrodes and estimation of percentage of electroactive Ru(II) on the NiO surface

Sample	Ru(ICP-MS)[a] (nmol cm^{-2})	Ru(CV)[b] (nmol cm^{-2})	Ru (CV) / Ru(ICP-MS)
NiO/PRu*Pyr*	6.2	2.0	0.32
NiO/PRu-*PolyPyr*-RuC$_2$bpy	30.2	9.6	0.32
NiO/PRu-*PolyPyr*-RuC$_2$RuCAT1	40.1	11.6	0.29
NiO/PRu-*PolyPyr*-RuC$_2$RuCAT2	16.3	4.4	0.27

[a] Total amounts of Ru complexes in each electrode, that were measured by using ICP-MS analysis. [b] Amounts of electroactive Ru complexes measure by using CV analysis.

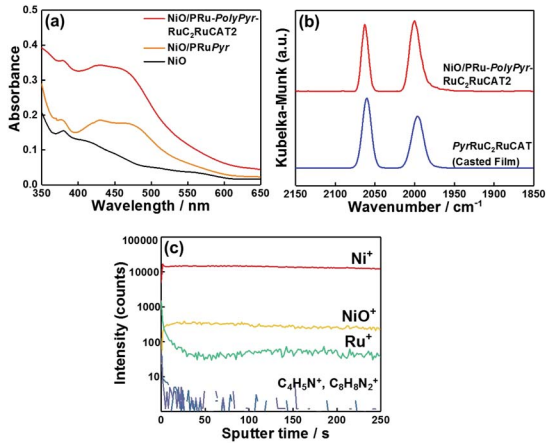

Fig. 7 (a) UV-Vis (DR) absorption spectra of NiO/PRu-*PolyPyr*-RuC_2-RuCAT2 (red), NiO/PRu*Pyr* (orange), and NiO (black). (b) FT-IR (DR) spectra of NiO/PRu-*PolyPyr*-RuC_2RuCAT2 (red) and *Pyr*RuC_2RuCAT cast on NiO (blue). (c) TOF-SIMS spectra of NiO/PRu-*PolyPyr*-RuC_2RuCAT2.

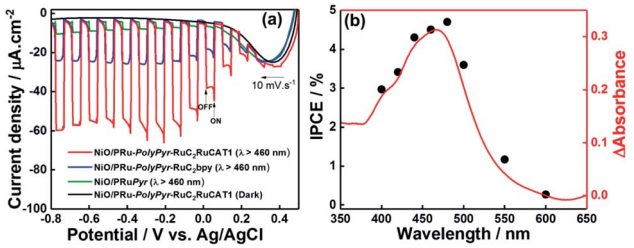

Fig. 8 (a) Responses of NiO/PRu*Pyr* (green), NiO/PRu-*PolyPyr*-RuC_2bpy (blue), and NiO/PRu-*PolyPyr*-RuC_2RuCAT1 (red) to irradiation at λ_{ex} = 460–650 nm (intensity = 28.2 mW cm^{-2}) in CO_2-purged 50 mM aqueous $NaHCO_3$ (pH 6.6, Ag/AgCl reference electrode, Pt wire counter electrode). (b) Effect of wavelength on the IPCE of NiO/PRu-*PolyPyr*-RuC_2RuCAT1 at −0.3 V *vs.* Ag/AgCl in a CO_2-purged 50 mM $NaHCO_3$ aqueous solution (pH 6.6, black dots). The red line shows the UV-vis absorption spectrum of NiO/PRu-*PolyPyr*-RuC_2-RuCAT1 with subtracted absorbance of the NiO electrode.

indicated that 8.2 nmol cm^{-2} of electrochemically active Ru complexes was immobilized on NiO, with the difference between the maxima of oxidation and reduction waves (ΔE) equaling 51 mV. The polymerization of metal complexes initiated by the oxidation of pyrrole group(s) should initiate the binding of Ru(II) complexes through C–C bond formation between the pyrrole groups, and the propagation of this process should generate a polypyrrole layer containing Ru(II)trisdiimine complex units on the electrode surface to form a Ru complex-based dye-coated NiO/*PolyPyr*Ru electrode. The singlet metal-to-ligand charge transfer (^{1}MLCT) absorption band of the Ru complex dye units was clearly observed in the UV-vis diffuse reflectance (DR) spectrum of NiO/*PolyPyr*Ru (Fig. 1e). Scanning electron microscopy (SEM) images of the electrodes before and after polymerization suggested that the electropolymerization of metal complex units occurred not only on the surface of the NiO electrode but also on deeper-lying NiO particles (Fig. 2c).

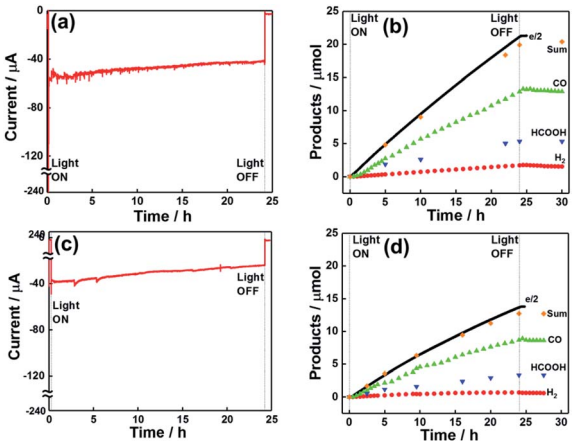

Fig. 9 Time courses of (a and c) photocurrent and (b and d) product levels expressed as half of electrons passed (black line), CO (green triangles), HCOOH (blue triangles), and H_2 (red circles). (a and b) NiO/PRu-*PolyPyr*-RuC_2RuCAT1, (c and d) NiO/PRu-*PolyPyr*-RuC_2RuCAT2 (electrode area = 2.5 cm^2, applied bias (E) = −0.7 V *vs.* Ag/AgCl) were irradiated at λ_{ex} = 460–650 nm (32 mW cm^{-2}) in CO_2-purged 50 mM aqueous $NaHCO_3$ (pH 6.6).

Although an increase in the sweep number to 50 (Fig. 1c) increased the amount of electrode-deposited Ru(II) complexes (14.4 nmol cm^{-2}, Fig. 1d), it also increased the difference between the peaks of the oxidation and reduction waves (ΔE = 83 mV, *cf.* ΔE = 51.0 mV for 25 sweeps), *i.e.*, electron mobility concomitantly decreased. The responses of the *I–V* curves of the polymer electrodes to visible light were investigated in CO_2-purged aqueous solutions containing 50 mM $NaHCO_3$ as the electrolyte (Fig. 1f), and the photocurrent density (16.7 μA cm^{-2}) of the electrode prepared by 25 sweeps exceeded that of the electrode prepared using 50 sweeps. These results clearly indicate that the sweep number of 25 is more suitable for molecular photoelectrode fabrication *via* pyrrole polymerization.

Fig. S2† shows the results obtained using *Pyr*2Ru as the starting complex and 25 sweeps between E = 0 and +1.35 V, revealing that the number of electrochemically active Ru complexes on the electrode exceeded that observed when *Pyr*Ru was used as the starting complex. However, upon irradiation, the former electrode afforded a lower photocurrent than the latter. The large ΔE of the electrode prepared from *Pyr*2Ru (ΔE = 133 mV) also indicated that the electron mobility of the corresponding polymer was lower than that of the polymer prepared from *Pyr*Ru. These results provided useful guidance for the fabrication of molecular photoelectrodes from NiO and Ru(II) trisdiimine complexes connected with polypyrrole moieties, suggesting that the optimal conditions correspond to the use of Ru(II) complexes with only one *Pyr*bpy ligand and 25 sweeps between E = 0 and +1.35 V. Therefore, these polymerization conditions were chosen for subsequent experiments.

Preparation of dye-sensitized molecular photocathodes

Scheme 3 presents three Ru(II) complexes prepared to develop two kinds of polypyrrole-based dye-sensitized molecular photocathodes. PRu*Pyr* has three different diimine ligands,

Table 3 Photoelectrochemical CO_2 reduction performances of photocathodes under various conditions

Entry	Electrode	Irradn time (h)	E_{app} [a] (V)	Light intensity (mW cm^{-2})	Products/μmol (TON) CO	HCOOH	H_2	F_{red} [b] (%)	CO_2 red selectivity (%)
1	NiO/PRu-*PolyPyr*-RuC_2RuCAT1	5	−0.7	32	3.8 (152.6)	1.0 (40.2)	0.4 (16.1)	91	93
2		24	−0.7	32	14.1 (566.3)	4.6 (184.7)	1.8 (72.3)	96	92
3		24	−0.3	27	5.2 (208.8)	2.9 (116.5)	1.0 (40.2)	91	89
4		24	0.0	28	2.2 (88.4)	2.1 (84.3)	0.9 (36.1)	71	82
5		24	−0.7	8	4.9 (196.8)	3.2 (128.5)	1.1 (44.2)	87	89
6	NiO/PRu-*PolyPyr*-RuC_2RuCAT2	24	−0.7	36	7.8 (619)	3.4 (269.8)	1.4 (111.1)	93	89
7	NiO/PRu-*PolyPyr*-RuC_2RuC_2bpy	5	−0.7	36	0.1	0.1	1.1	92	19
8	NiO/*PolyPyr*-RuC_2RuCAT[c]	5	−0.7	32	0.2	0.6	<0.1	83	91
9	NiO/PRu*Pyr*	5	−0.7	32	n.d.[d]	n.d.[d]	<0.1	9	n.d.[d]
10[e]	NiO/PRuC_2RuCAT	5	−0.7	27	<0.1	0.2	<0.1	56	82

[a] Applied potential *vs.* Ag/AgCl. [b] Faradaic efficiency of the total production of CO, HCOOH. [c] Without process 1. [d] Not detected. [e] Reference [12].

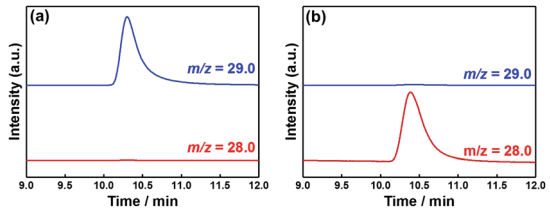

Fig. 10 GC-MS chromatograms of the gas phase formed in cells after irradiation, showing the peaks at m/z = 28 and 29 (^{12}CO and ^{13}CO, respectively). NiO/PRu-*PolyPyr*-RuC_2RuCAT1 was subjected to an applied bias of E = −0.7 V *vs.* Ag/AgCl and irradiated at λ_{ex} = 460–650 nm in CO_2-purged 50 mM aqueous $NaHCO_3$ (pH = 6.6) for 24 h using (a) $^{13}CO_2$ and $NaH^{13}CO_3$ and (b) ordinary CO_2 and $NaHCO_3$.

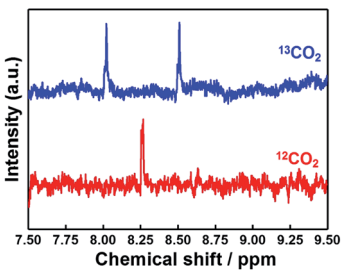

Fig. 11 ^1H NMR spectra of the solution obtained after photoelectrochemical reduction. NiO/PRu-*PolyPyr*-RuC_2RuCAT1 was subjected to a potential of E = −0.7 V *vs.* Ag/AgCl and irradiated at λ_{ex} = 460–650 nm in CO_2-purged 50 mM aqueous $NaHCO_3$ (pH = 6.6) for 24 h using $^{13}CO_2$ and $NaH^{13}CO_3$ (blue) or ordinary CO_2 and $NaHCO_3$ (red).

namely [2,2′-bipyridine]-4,4′-diylbis(phosphonic acid) ($(H_2O_3PCH_2)_2$bpy, anchor to the NiO electrode), dmb, and *Pyr*bpy. One of the other two Ru(II) complexes was dissolved in MeCN and polymerised with the PRu*Pyr* attached to the NiO electrode to form a polypyrrole layer. *Pyr*RuC_2bpy has a free diimine moiety that can react with other metal ions after polymerization to introduce the catalyst unit, while *Pyr*RuC_2RuCAT is a supramolecular photocatalyst bearing both redox photosensitizer Ru(II) and catalytic Ru(II) units connected to each other *via* an ethylene chain.

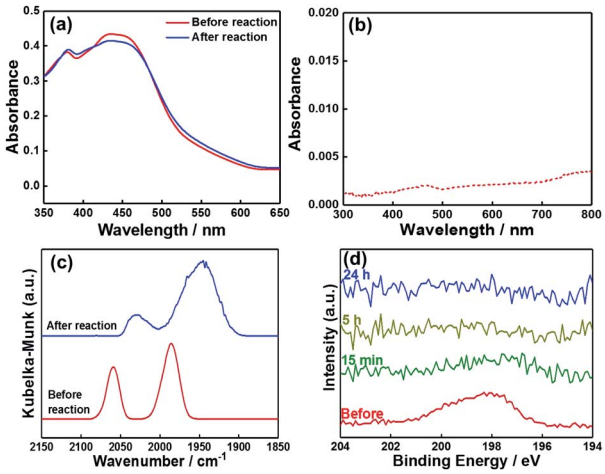

Fig. 12 (a) UV-Vis DR spectra of NiO/PRu-*PolyPyr*-RuC_2RuCAT1 before (red) and after (blue) photoelectrochemical CO_2 reduction (−0.7 V *vs.* Ag/AgCl, λ_{ex} = 460–650 nm, 24 h) in CO_2-purged 50 mM aqueous $NaHCO_3$. (b) UV-vis absorption spectrum of the reaction solution after the photocatalytic reaction. (c) FT-IR (DR) spectra of NiO/PRu-*PolyPyr*-RuC_2RuCAT1 before (red) and after (blue) the photocatalytic reaction. (d) Cl 2p spectra of NiO/PRu-*PolyPyr*-RuC_2-RuCAT1 before and after the photocatalytic reaction for various times.

A three-step method was used to prepare NiO/PRu-*PolyPyr*-RuC_2RuCAT1 as a dye-sensitized molecular photocathode (Scheme 4 and Fig. S3†). The NiO electrode was first modified with PRu*Pyr* to give NiO/PRu*Pyr*, in which the methylphosphonic acid groups of the diimine ligand work as anchors to the NiO electrode (process 1) (Scheme 4a). In the second step, NiO/PRu*Pyr* was used as the working electrode for the oxidative electropolymerization of *Pyr*RuC_2bpy dissolved in MeCN containing Et_4NBF_4 (0.1 M) as an electrolyte (process 2) (Scheme 4b). Oxidative cyclic voltammetry cycling was carried out 25 times between E = 0 and +1.35 V *vs.* Ag/$AgNO_3$ at 100 mV s^{-1}, and the gradual increase of redox wave intensity after each scan (Fig. 3a) indicated the development of a polymer layer on the electrode to give NiO/PRu-*PolyPyr*-RuC_2bpy. Finally, NiO/PRu-*PolyPyr*-RuC_2bpy with free diimine moieties was reacted with $[Ru(CO)_2Cl_2]_n$ in MeCN solution at room temperature to give

Table 4 Photoelectrochemical CO_2 reduction performances of NiO/PRu-*PolyPyr*-RuC_2RuCAT1 electrodes prepared by different number of potential sweeps for polymerization, with other electrode production and photocatalytic reaction parameters held constant

Entry	Number of sweeps	$e^-/2$ μmol	Product/μmol CO	HCOOH	H_2	F_{red} (%)	CO_2 red. selectivity (%)
1	5	0.99	0.2	0.4	0.1	77	70
2	10	1.69	0.6	0.6	0.1	83	90
3	20	4.12	2.5	1.0	0.3	91	93
4	25	4.89	2.9	1.0	0.3	91	92
5	50	2.99	2.0	0.7	0.2	97	94
6	Fixed[a]	1.35	0.6	0.6	0.1	94	91
7	25[b]	0.95	0.2	0.6	<0.1	83	91

[a] Electrolysis for the polymerization was performed at 1.3 V *vs.* Ag/$AgNO_3$ for 30 min. [b] Without using PRu*Pyr* to make the photocathode.

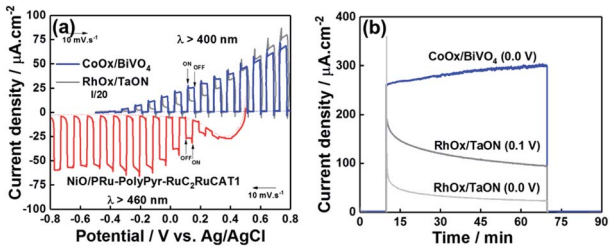

Fig. 13 (a) *I–V* curves of $CoO_x/BiVO_4$, RhO_x/TaON, and NiO/PRu-*PolyPyr*-RuC_2RuCAT1 as working electrodes recorded in CO_2-purged aqueous $NaHCO_3$ (50 mM) upon irradiation. Scan rate = 10 mV s^{-1}, λ_{ex} = 400–650 nm (41 mW cm^{-2}) for $CoO_x/BiVO_4$ and RhO_x/TaON, and λ_{ex} = 460–650 nm (28mW cm^{-2}) for NiO/PRu-*PolyPyr*-RuC_2RuCAT1. (b) Time-dependent photocurrents of $CoO_x/BiVO_4$ at E_{app} = 0 V (blue) and RhO_x/TaON at *E* = 0 V (light grey) and 0.1 V (dark grey) *vs.* Ag/AgCl.

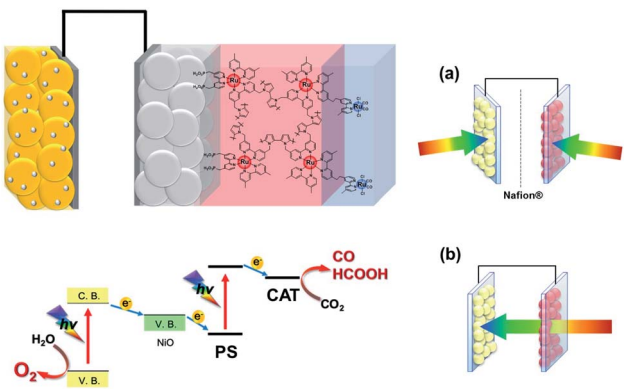

Scheme 5 Schematics of a full cell comprising a $CoO_x/BiVO_4$ or RhO_x/TaON photoanode and a NiO/PRu-*PolyPyr*-RuC_2RuCAT1 photocathode. (a) Irradiation of a full cell with two compartments separated by a Nafion® membrane. (b) Tandem-type full cell with a single compartment.

NiO/PRu-*PolyPyr*-RuC_2RuCAT1 with Ru(diimine)$(CO)_2Cl_2$-type complexes in the polypyrrole layer as catalytic units (process 3) (Fig. S3†) (Scheme 4c).

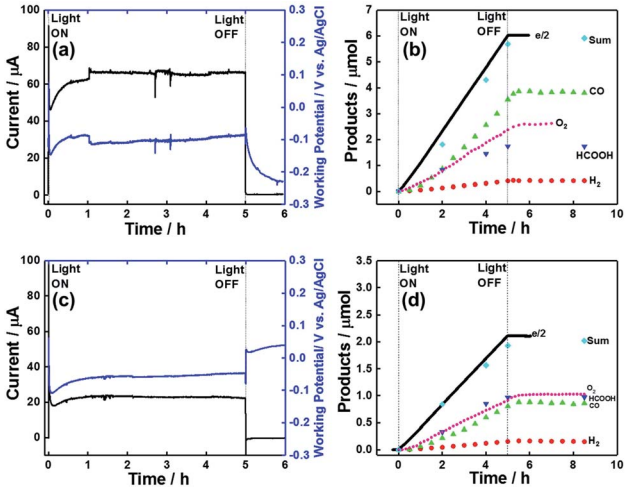

Fig. 14 (a and c) Time courses of electrode photocurrent (black) and working potential (blue), and (b and d) product amounts formed during visible light irradiation. Data recorded for photoelectrochemical cells with the NiO/PRu-*PolyPyr*-RuC_2RuCAT1 photocathode and (a and b) the $CoO_x/BiVO_4$ photoanode (photocathode: λ_{ex} = 460–650 nm, 32 mW cm^{-2}, photoanode: λ_{ex} = 400–650 nm, 28 mW cm^{-2}) or (c and d) the RhO_x/TaON photoanode (photocathode: λ_{ex} = 460–650 nm, 34.4 mW cm^{-2}, photoanode: λ_{ex} = 400–650 nm, 32.2 mW cm^{-2}) without any bias in aqueous CO_2-purged $NaHCO_3$ (50 mM, pH 6.6).

The synthesized electrodes were characterized by cyclic voltammetry (Fig. 3b and d), spectrophotometry, time-of-flight secondary ion mass spectrometry (TOF-SIMS), X-ray photoelectron spectroscopy (XPS), and SEM-based morphological analysis.

Fig. 4a shows the UV-vis DR spectra of NiO/PRu-*PolyPyr*-RuC_2RuCAT1, revealing an increase in the intensity of the ^{1}MLCT absorption band of Ru complexes after polymerization (process 2), while no such increase was observed after the formation of Ru catalyst units (process 3). This is reasonable, as Ru(diimine)$(CO)_2Cl_2$-type complexes have no strong absorption at wavelengths above 350 nm.[12] The Fourier transform infrared (FT-IR) DR spectrum of NiO/PRu-*PolyPyr*-RuC_2RuCAT1 showed two strong broad peaks at 2058 and 1986 cm^{-1}, which were attributed to the C=O stretches of CO ligands in catalyst units, whereas no such peaks were observed for NiO/PRu-*PolyPyr*-RuC_2bpy (Fig. 4b). The CO stretching frequencies well agreed with those of the corresponding binuclear Ru(II) complex ([*cis*-(CO)-*trans*-(Cl)-Ru$(CO)_2Cl_2$(bpyC$_2$bpy)Ru(dmb)$_2$]$(PF_6)_2$ (bpyC$_2$bpy = 1,2-bis(4′-methyl-[2,2′-bipyridine]-4-yl)ethane)) drop-cast on the NiO electrode (2058 and 1991 cm^{-1}).[12] Fig. 4c and d show the X-ray photoelectron spectra of NiO/PRu-*PolyPyr*-RuC_2RuCAT1 with the Ru catalyst unit and catalyst-free NiO/PRu-*PolyPyr*-RuC_2bpy. Although both compounds featured a Ru 3d peak at 281.1 eV (Fig. 4c), only NiO/PRu-*PolyPyr*-RuC_2RuCAT1 showed a Cl 2p peak at 198.4 eV (Fig. 4d). These results suggested that the Ru(II) catalyst units on and/or in the polypyrrole polymer on the electrode existed predominantly in the form of *cis*-(CO)-*trans*-(Cl)-Ru(diimine)$(CO)_2Cl_2$, which has been investigated as a catalyst for CO_2 reduction in various photo- and electrocatalytic reactions.[48–50]

Table 5 Photocatalytic performances of full-cell devices in CO_2-purged 50 mM $NaHCO_3$

Photo-anode	Light intensity (mW cm^{-2})	Irradn time (h)	Products/μmol					$F_{cathode}$ (%)	F_{anode} (%)	CO_2 red. selectivity (%)	ECE (10^{-2}%)
			$e^-/2$	CO	HCOOH	H_2	O_2				
Two-component systems											
CoO_x/$BiVO_4$	32.0[a], 28.0[b]	5	6.0	3.9	1.7	0.4	2.6	99	87	93	8.3
RhO_x/TaON	34.4[a], 32.2[b]	5	2.1	0.9	1.0	0.2	1.0	96	97	92	2.0
One-component systems											
CoO_x/$BiVO_4$	100[c]	1	1.6	0.6	0.9	0.1	0.6	98	74	92	4.8
RhO_x/TaON	100[c]	1	1.0	0.4	0.5	<0.1	0.5	95	96	95	2.7

[a] At λ_{ex} = 460–650 nm for photocathode. [b] At λ_{ex} = 400–650 nm for photoanode. [c] AM1.5.

The SEM images of NiO/PRu-*PolyPyr*-RuC_2RuCAT1 and the bare NiO electrode reveals that polypyrrole-containing Ru complex units formed not only on the surface of the NiO electrode but also inside the NiO layer (Fig. 2a and d). The Ru complexes could sufficiently penetrate into the depth of electrodes owing to the porosity of the NiO electrode.

Fig. 5 shows the results of TOF-SIMS analysis, indicating the distribution of elements in the depth direction from the electrode surface, with the sputter time on the *x*-axis corresponding to the cross-sectional component in the depth direction.

Although the density of Ru^+ species on the electrode surface was highest for NiO/PRu-*PolyPyr*-RuC_2RuCAT1, a relatively high intensity of these species was observed throughout the entire range of the NiO layer. This finding supports the conclusion that Ru complex units were fixed not only on the surface of the electrode, but also within its interior. Both the photosensitizer and catalyst moieties should be similarly dispersed on and in the NiO electrode because of the similarity of the TOF-SIMS spectra of NiO/PRu-*PolyPyr*-RuC_2RuCAT1 and NiO/PRu-*PolyPyr*-RuC_2bpy. A comparison of these spectra with that of NiO-PRu*Pyr* indicates that polymerization increased the number of Ru complex units, especially in the NiO layer. The densities of BF_4^- and Et_4N^+ in NiO/PRu-*PolyPyr*-RuC_2RuCAT1 were also measured using the TOF-SIMS analysis (Fig. S4†). BF_4^- was observed throughout the entire range of the NiO layer while no Et_4N^+ was detected. This indicates that remove of reductants ions were achieved by the post handling after the polymerization (Experimental section).

We determined the total amount of the adsorbed Ru complexes on each electrode by using the ICP-MS analysis. The results are summarized in Table 1. The amount of the photosensitizers clearly increased after the oxidative polymerization: the amount of Ru(II) photosensitizer of NiO/PRu-*PolyPyr*-RuC_2bpy (step-2) was 30.2 nmol cm^{-2} while that of NiO/PRu*Pyr* (after the step-1) was 6.2 nmol cm^{-2}. After incorporation of the catalysts into the polymer electrode a total amount of Ru complexes increase again to 40.1 nmol cm^{-2}. Therefore, the adsorbed amount of the Ru catalysts was 9.9 nmol cm^{-2} in the case of NiO/PRu-*PolyPyr*-RuC_2RuCAT1, which is about one third of the photosensitizers. This means about 14 nmol cm^{-2} of the free bpy units remained in NiO/PRu-*PolyPyr*-RuC_2RuCAT1. Limitation of space in the polypyrrole polymer might suppress the reaction of these bpy units with the precursor of the catalyst in the step 3.

The amounts of electrochemically active photosensitizers after each step were determined by cyclic voltammetric analysis of the film (Table 2).[27] The electroactive photosensitizers were also increased after each adsorption steps of the photosensitizers: 2.0 nmol cm^{-2} (NiO/PRu*Pyr*) and 9.6 nmol cm^{-2} (NiO/PRu-*PolyPyr*-RuC_2bpy). After the introduction of the catalysts, the amounts of electrochemically active photosensitizers slightly increased (11.6 nmol cm^{-2}, NiO/PRu-*PolyPyr*-RuC_2-RuCAT1) probably because of small morphology change of the polypyrrole phase during the reaction. The proportion of the electroactive photosensitizers to the total amount of the photosensitizers was about 0.3 (Table 2). Although this result indicates that major part of the immobilized photosensitizers was silent during the electrochemical scans, the non-electroactive photosensitizers possibly worked in the photocatalytic reactions owing to slower electron hoping than the time scale of the CV measurements and/or electron transfer in the excited state.

The stability of NiO/PRu-*PolyPyr*-RuC_2RuCAT1 in an aqueous solution containing 50 mM $NaHCO_3$ (this solution was used for photocatalytic CO_2 reduction, as described below) was checked by spectrophotometric and electrochemical analyses using NiO/PRu*Pyr* as a reference sample without polymerization. The voltammograms of NiO/PRu-*PolyPyr*-RuC_2RuCAT1 recorded before and after 24 h soaking in the above solution (Fig. 6a) indicated that much less than 5% of the electroactive Ru(II) complexes was detached from the electrode, whereas, in the case of NiO/PRu-*Pyr* (Fig. 6b), more than 70% of PRu*Pyr* adsorbed on the NiO electrode through methylphosphonic acid groups was detached into the aqueous solution. A much stronger immobilization of the Ru complex units in the polypyrrole layer on the electrode was also confirmed by spectrophotometric analysis. Specifically, the ^{1}MLCT absorption band in the UV-vis (DR) spectrum of NiO/PRu-*PolyPyr*-RuC_2RuCAT1 remained almost unchanged after soaking (Fig. 6c), and no Ru complexes were observed in the soaking solution (Fig. 6e). On the other hand, almost no ^{1}MLCT absorption was observed in the UV-vis (DR) spectrum of soaked NiO/PRu*Pyr*, and the absorption of dissolved PRu*Pyr* was observed in the corresponding soaking solution (Fig. 6d and f). These results indicated that the fixation of Ru complexes using

the polypyrrole layer is a very powerful means of preventing their detachment from the electrode in this solution.

Another dye-sensitized molecular photocathode (NiO/PRu-*PolyPyr*-RuC_2RuCAT2) was prepared by a simple two-step method. In this case, the NiO/PRu*Pyr* electrode was used as the working electrode for the oxidative electropolymerization of *Pyr*RuC_2RuCAT, which already has both photosensitizer and catalyst units, in MeCN containing Et_4NBF_4 (0.1 M) as an electrolyte. Oxidative cyclic voltammetry cycling was performed between 0 and +1.35 V *vs.* Ag/$AgNO_3$ at 100 mV s^{-1} (Scheme 4a and d), *i.e.*, under the same polymerization conditions as those used for NiO/PRu-*PolyPyr*-RuC_2RuCAT1. The voltammograms recorded during electrochemical polymerization (Fig. 3c) resembled those obtained after process 2 using *Pyr*RuC_2bpy (Fig. 3a). This is reasonable, as the oxidation potential of the incorporated catalyst unit is more positive than that of the pyrrole groups (Fig. S5†). In other words, the catalyst unit incorporation did not affect the oxidative polymerization of pyrrole groups. We can use the amounts of the Ru complexes in NiO/PRu*Pyr* and NiO/PRu-*PolyPyr*-RuC_2RuCAT2, which were obtained by using the ICP-MS analysis, to determine both amounts of the photosensitizers and catalysts in NiO/PRu-*PolyPyr*-RuC_2RuCAT2 because we can assume that the adsorbed amounts of the photosensitizer and catalyst units to NiO/PRu-*Pyr* (step 2 in the two-step method) was same to each other because the Ru(II)–Ru(II) supramolecule with the 1 : 1 ratio between the photosensitizer and catalyst units was used as the monomer for the polymerization. These results are summarized in Table 1. Both amounts of the adsorbed photosensitizers and the catalysts in NiO/PRu-*PolyPyr*-RuC_2RuCAT2 were less than half of those in NiO/PRu-*PolyPyr*-RuC_2RuCAT1. This difference was ascribed to the much higher bulkiness of the RuCAT unit of *Pyr*RuC_2RuCAT compared to that of the free diimine unit of *Pyr*RuC_2bpy, which possibly suppressed the supply of *Pyr*RuC_2RuCAT to NiO particles at the electrode depth. The number of active Ru complexes in NiO/PRu-*PolyPyr*-RuC_2RuCAT2 estimated by cyclic voltammetry of the polymer electrode (4.4 nmol cm^{-2}, Fig. 3d) was smaller than that of the electrode prepared using the abovementioned three-step method (11.6 nmol cm^{-2}, Fig. 3b).

In the case of NiO/PRu-*PolyPyr*-RuC_2RuCAT2, similar structures and stabilities of Ru complex units in the polypyrrole layer were confirmed by UV-vis DR spectroscopy (Fig. 7a), FT-IR spectroscopy (Fig. 7b), TOF-SIMS (Fig. 7c), and SEM (Fig. 2b). Notably, the catalytic unit with the *cis*-(CO)-*trans*-(Cl)-Ru(diimine)$(CO)_2Cl_2$ structure did not change during oxidative polymerization. This is one of critical differences of the oxidative polymerization method of the pyrrole groups from the previously reported reductive polymerization method using a similar Ru(II)–Ru(II) supramolecular photocatalyst with vinyl groups instead of the pyrrole groups, noticeable shifts in CO stretching frequencies were observed after the reductive polymerization.[12] This finding suggested the formation of Ru–C bonds during the reductive polymerization, which induced the desorption of complexes from the electrode during photocatalytic reactions.[12] Such decomposition process of the photoanode was not observed in the system using NiO/PRu-*PolyPyr*-RuC_2RuCAT2.

Photoresponses of dye-sensitized molecular photocathodes

Fig. 8a presents the *I–V* curve (linear sweep voltammogram) of NiO/PRu-*PolyPyr*-RuC_2RuCAT1 recorded during irradiation at λ_{ex} = 460–650 nm in CO_2-purged aqueous 50 mM $NaHCO_3$ as the electrolyte, revealing a photocathodic current response starting from E = +0.4 V *vs.* Ag/AgCl. The photocurrent steadily increased up to E = −0.2 V, saturating at more negative potentials. This photocurrent increase was faster than that of a previously reported NiO/PRu-*PolyVinyl*-RuC_2RuCAT photocathode[12] prepared by a similar three-step method except for the reductive polymerization of the vinyl groups of the Ru photosensitizer units instead of the oxidative polymerization of the pyrrole groups. Specifically, the maximum photocurrent (61 μA cm^{-2}) was achieved even at E = −0.2 V in the case of NiO/PRu-*PolyPyr*-RuC_2RuCAT1, whereas E = −0.5 V was required to maximize the photocurrent of NiO/PRu-*PolyVinyl*-RuC_2RuCAT (28.0 μA cm^{-2} at E = −0.2 V, 38.0 μA cm^{-2} at E = −0.5 V). At E = 0 V, NiO/PRu-*PolyPyr*-RuC_2RuCAT1 maintained ∼83% of the maximum photocurrent density, whereas this number equalled only 45% for NiO/PRu-*PolyVinyl*-RuC_2RuCAT. These results strongly indicated that the electric resistance of the polypyrrole layer in NiO/PRu-*PolyPyr*-RuC_2RuCAT1 was lower than that of the polyvinyl layer in NiO/PRu-*PolyVinyl*-RuC_2RuCAT.

The dependence of IPCE on the wavelength of irradiated light (Fig. 8b) well agreed with the behaviour of the ^{1}MLCT absorption band of Ru complex photosensitizer moieties. Therefore, the cathodic photocurrent was exclusively generated by the excitation of Ru photosensitizer moieties in the polymerized layer on the NiO electrode. The maximum IPCE (4.7% at λ_{ex} = 480 nm) was approximately four times higher than that of a previously reported system with NiO/PRu-*PolyVinyl*-RuC_2RuCAT (IPCE = 1.2%).[12]

The responses of photocathodes obtained after each fabrication step were observed at E = −0.7 V and equaled 9.8 μA cm^{-2} for NiO/PRu*Pyr* prepared by process 1 and 24.5 μA cm^{-2} for NiO/PRu-*PolyPyr*-RuC_2bpy prepared by process 2. Both of these values were much lower than that observed for NiO/PRu-*PolyPyr*-RuC2RuCAT1 (57 μA cm^{-2}).

Photoelectrochemical CO_2 reduction over dye-sensitized molecular photocathodes

The photocatalytic activity of dye-sensitized molecular photocathodes for CO_2 reduction under external bias was evaluated using them as working electrodes and Pt wire as a counter electrode. These electrodes were set in each compartment of an H-shaped cell, in which the compartments were separated using a Nafion® membrane, and a Ag/AgCl (Sat. KCl aq.) KCl reference electrode was set in the same compartment as the dye-sensitized molecular photocathode. Aqueous 50 mM $NaHCO_3$ as the electrolyte was introduced into the cell and purged with CO_2 for 30 min. The compartment with the dye-sensitized photocathode was irradiated at λ_{ex} = 460–650 nm using a 300 W Xe lamp with a cutoff filter under applied biases of E_{app}

= 0, −0.3, and −0.7 V. During irradiation, CO_2 flowed into the solution, and the flow gas was analysed by a micro-GC to determine the levels of the produced CO and H_2. The reaction solution was sampled using a syringe through a septum cap attached to the cathodic compartment. Fig. 9a shows the irradiation time–dependent photocurrent at $E_{app} = -0.7$ V in the system with NiO/PRu-*PolyPyr*-RuC_2RuCAT1 as the photocathode, revealing that a continuous photocathodic current of 57 to 43 μA was observed over 24 h. CO and HCOOH were continuously formed as major products along with small amounts of H_2 (Fig. 9b). The CO_2 reduction selectivity equalled 92%, while the faradaic efficiency (F_{red}) of this reduction equalled 96% after 24 h irradiation, even though the photocatalytic reaction proceeded in an aqueous solution with pH 6.8. The product turnover numbers after 24 h irradiation equalled 566.3 (CO), 184.7 (HCOOH), and 72.3 (H_2) (entry 2 in Table 3), and the number of Ru catalyst moieties was estimated by ICP-MS analysis as 24.9 nmol (see experimental).

Control experiments performed without irradiation, without applied potential, or under an Ar atmosphere using phosphate buffer (pH 7.4) instead of $NaHCO_3$ as an electrolyte gave no or less CO_2 reduction products (Table S5†), suggesting that light, applied bias, and CO_2 are required for photocatalytic CO_2 reduction. Compared to NiO/PRu-*PolyPyr*-RuC_2RuCAT1, the catalyst unit–free NiO/PRu-*PolyPyr*-RuC_2bpy showed no significant activity for CO_2 reduction but afforded some H_2 upon irradiation (entry 7 in Table 3), which indicated that the Ru catalyst unit is essential for the photocatalytic reduction of CO_2 in this photoelectrochemical system.

Fig. 10a shows a GC-MS chromatogram of the gas phase formed in the photocathode compartment after 24 h irradiation of the system containing $^{13}CO_2$ and $NaH^{13}CO_3$, indicating the almost selective formation of ^{13}CO ($m/z = 29$). On the other hand, a similar experiment with ordinary CO_2 and $NaHCO_3$ afforded a main peak at $m/z = 28$ (^{12}CO; Fig. 10b). Fig. 11 shows the ^1H NMR spectra of the reaction solution formed in the cathodic compartment after irradiation. In the case of $^{13}CO_2$ and $NaH^{13}CO_3$, a doublet attributable to $H^{13}COO^-$ was observed at 8.26 ppm ($J_{CH} = 196$ Hz) because of ^1H–^{13}C coupling, while a singlet was observed at 8.26 ppm for the system with ordinary CO_2 and $NaHCO_3$. These isotope labelling experiments confirmed that CO_2 acted as a source of carbon in the photocatalytic reduction products (CO and HCOOH).

After the photocatalytic reaction, the photocathode was analysed by UV-vis DR spectroscopy, FT-IR (DR) spectroscopy, and XPS. Almost no changes were observed in the UV-vis DR spectra after the reaction (Fig. 12a), and no desorbed Ru(II) trisdiimine complexes were observed in the reaction solution (Fig. 12b). These results indicate that the Ru(II) photosensitizer units were stable and that the polypyrrole layer was strong enough to keep the Ru photosensitizer units in its layer during the photocatalytic reaction for at least one day. Fig. 12c shows the expanded FT-IR (DR) spectra depicting the ν_{CO} bands before and after the reaction. Although these bands were still observed after the reaction, they were shifted to lower wavenumbers (ν_{CO} = 1945, 2030 cm^{-1}), which suggest that the Cl^- ligands of Ru catalyst units were replaced with electron-donating ligands such as OH^- or $HCOO^-$. The exchange of Cl^- ligands during the photocatalytic reaction was further confirmed by the disappearance of the Cl 2p peaks in the X-ray photoelectron spectra (Fig. 12d), which indicate that the loss of Cl^- mostly proceeded within the initial 15 min of the photocatalytic reaction. As the concentration change of Ru catalyst units could not be determined, one cannot discuss the reason(s) of why the photocatalytic reaction rate decreased with time, even though it remained at 76% of the initial value after 24 h (Fig. 9a).

The formation of reduction products became slower at lower applied potentials, *i.e.*, at $E_{app} = -0.3$ and 0 V (entries 3 and 4 in Table 3), even though the photocurrents at $E_{app} \leq -0.2$ V were similar (Fig. 8). The back electron transfer from the reduced Ru complex units to the electrode might have proceeded more efficiently at $E_{app} = -0.3$ V than at $E_{app} = -0.7$ V. It should be noted, however, that photocatalytic CO_2 reduction still actively proceeded even at $E_{app} = 0$ V. Interestingly, the HCOOH : CO ratio at these lower applied potentials exceeded that obtained at $E_{app} = -0.7$ V (entry 2 in Table 3). A similar change in reduction product ratio, that is, a decrease in the fraction of CO, was observed with decreasing irradiation intensity (32 → 8 mW cm^{-2}) even at $E_{app} = -0.7$ V (entries 2 and 5 in Table 3 and Fig. S6†). These results suggest that slower electron injection into the catalyst units favours the formation of HCOOH. Ishida *et al.* reported a similar phenomenon in homogeneous solutions, *i.e.*, the HCOOH : CO ratio increased with decreasing irradiation intensity in the homogeneous photocatalytic reduction of CO_2 promoted by a mixture of $Ru(bpy)(CO)_2Cl_2$ and $[Ru(bpy)_3]^{2+}$ (bpy = 2,2′-bipyridine), and proposed that slower injection into the one-electron-reduced intermediate produced from the Ru catalyst induces the formation of a Ru catalyst dimer, with further reduction affording HCOOH.[51] Kubiak *et al.* proposed that in the electrocatalytic reduction of CO_2 using $Ru(6Mesbpy)(CO)_2Cl_2$, the bpy ligand of which has bulky mesityl groups at 6,6′-positions to suppress dimerization, slower electron injection into a Ru(II) formate complex as an intermediate of both CO and HCOOH formation induces the loss of the formate ligand from the Ru catalyst unit.[52] Although we cannot clarify the real reason of why faster electron injection into the Ru catalyst unit favours CO production, we note that the selectivity for CO_2 over H_2 remained high even in slower-electron-injection systems.

Subsequently, we determined the optimal number of potential sweeps in the polymerization of *Pyr*RuC_2bpy with NiO/PRu*Pyr* (process 2) for the photocatalytic reduction of CO_2 (Fig. S7,† Table 4). The best performance was obtained for the photoelectrode prepared by 25 sweeps (entry 4, Table 4), in good agreement with the electrochemical properties of the photoelectrodes described in the section "Optimization of redox photosensitizer layer on electrodes." Notably, the photoelectrode prepared by continuous electrolysis at a fixed potential (1.3 V *vs.* $Ag/AgNO_3$) for 30 min exhibited poor photocatalytic performance (entry 6, Table 4).

To check the necessity of the first process of NiO/PRu-*Poly-Pyr*-RuC_2RuCAT1 fabrication (process 1), we performed the direct polymerization of *Pyr*RuC_2bpy on the NiO electrode without PRu*Pyr* using 25 potential sweeps between 0 and

+1.35 V *vs.* $Ag/AgNO_3$ at 100 mV s^{-1}, and the electrode was then reacted with $[Ru(CO)_2Cl_2]_n$ in MeCN solution at room temperature, as in processes 2 and 3 for the synthesis of NiO/PRu-*PolyPyr*-RuC_2RuCAT1 (entry 7 in Table 4).

Although this photocathode without phosphonic acid anchoring groups showed a certain photoresponse, its photocatalytic activity was much poorer than that of NiO/PRu-*PolyPyr*-RuC_2RuCAT1 (entry 7 in Table 4). Therefore, process 1 was concluded to be important for the synthesis of an efficient dye-sensitized molecular photocathode.

Fig. 9c and d show the photocatalytic performance of the system with NiO/PRu-*PolyPyr*-RuC_2RuCAT2 as a photocathode under an applied bias of −0.7, revealing the continuous production of CO and HCOOH as the main products for 24 h. The faradaic efficiency of reduction was 93% after 24 h. As the number of Ru catalyst units in this photoelectrode (12.6 nmol) was much smaller than that in NiO/PRu-*PolyPyr*-RuC_2RuCAT1 (24.9 nmol), the amount of reduction products was also smaller in the former system. However, the TONs obtained for NiO/PRu-*PolyPyr*-RuC_2RuCAT2 (entry 6 in Table 3) exceeded those obtained for NiO/PRu-*PolyPyr*-RuC_2RuCAT1 (entry 2 in Table 3).

In conclusion of this section, both NiO/PRu-*PolyPyr*-RuC_2RuCAT1 and NiO/PRu-*PolyPyr*-RuC_2RuCAT2 were found to be good dye-sensitized molecular photocathodes for photocatalytic CO_2 reduction, exhibiting high selectivity, durability, and faradaic efficiency and featuring IPCEs much higher ($IPCE_{max}$ = 4.7%) and onset potentials more positive than those of previously reported dye-sensitized molecular photocathodes ($IPCE_{max}$ < 2%)[11,12,19,27] such as NiO/PRu-*PolyVinyl*-RuC_2RuCAT with a polyvinyl polymer layer instead of the polypyrrole layer.[12] The faster electron hopping through the conjugated polypyrrole assembly should generate a higher photocurrent density at a lower bias in comparison with the polyvinyl-based electrodes. Therefore, polypyrrole systems are highly promising for the fabrication of good full-cell devices that drive photocatalytic CO_2 reduction using water as the reductant under zero bias conditions with visible light irradiation as the only energy input. Owing to the faster speed of product formation, we chose NiO/PRu-*PolyPyr*-RuC_2RuCAT1 as a photocathode for constructing full cells as follows.

Full cells for photocatalytic CO_2 reduction coupled with water oxidation

We chose two types of photoanodes, *i.e.*, $BiVO_4$ modified with CoO_x as a co-catalyst ($CoO_x/BiVO_4$)[53,54] and TaON modified with RhO_x as a co-catalyst (RhO_x/TaON),[55] as they were reported as stable semiconductor photoanodes for water oxidation under visible light irradiation with sufficient stability and sufficiently negative conduction band potentials to pass electrons to the valence band of NiO.[56,57] The photoelectrochemical properties of $CoO_x/BiVO_4$ and RhO_x/TaON were first checked by measuring their light responses (λ_{ex} = 400–650 nm, 41.2 mW cm^{-2}) (Fig. 13a, blue and gray lines), and in both cases, we observed good overlaps with the *I–V* curve of the NiO/PRu-*PolyPyr*-RuC_2RuCAT1 photocathode (red line) in CO_2-purged aqueous solutions containing 50 mM $NaHCO_3$ as the electrolyte (pH = 6.6). Therefore, the above electrodes were then used for photocatalytic CO_2 reduction. Relatively stable photocurrents continuously flowed in both photoanodes under low applied biases (E_{app} = 0 or 0.1 V *vs.* Ag/AgCl) and visible light irradiation in the same solutions (Fig. 13b and S8†). We used two types of photoelectrochemical cells with the NiO/PRu-*PolyPyr*-RuC_2RuCAT1 photocathode and the $CoO_x/BiVO_4$ or RhO_x/TaON photoanode. One type of cells featured a two-compartment system where the photocathode and the photoanode were separated from each other by a Nafion® membrane and were irradiated using different light sources (32–34 mW cm^{-2} at λ_{ex} = 460–650 nm for the photocathode, 28–32 mW cm^{-2} at λ_{ex} = 400–650 nm for the photoanode (Scheme 5a). In cells of the other (tandem) type, both photoelectrodes were set in the same compartment. Simulated solar light (AM1.5) first illuminated the photocathode, and then the permeated light illuminated the photoanode (Scheme 5b, Fig. S9 and S10†). No external bias was applied to the photoelectrodes in either cell type, that is, visible light was the only energy source.

Fig. 14a shows the time courses of the electrode photocurrent and working potential in the two-component system with the $CoO_x/BiVO_4$ photoanode, revealing that they were stable during 5 h irradiation. During this irradiation, CO and HCOOH were constantly produced in the photocathodic compartment, while O_2 was produced in the photoanodic compartment (Fig. 14b). The following results were obtained after 5 h: CO (3.90 μmol, TON_{CO} = 156.6), HCOOH (1.82 μmol, TON_{HCOOH} = 73.1), and O_2 (2.60 μmol). The much lower amount of produced H_2 (0.42 μmol) indicated high selectivity for CO_2 reduction (93%). The faradaic efficiencies of the photocathode and photoanode equaled 99 and 87%, respectively. The highest energy conversion efficiency obtained in the reported full cells with dye-sensitized molecular photocathodes equaled 8.3 × 10^{-2}% (Table 5). The full cell with the RhO_x/TaON photoanode also drove the photocatalytic reduction of CO_2 with water (Fig. 14c and d). The main product were also CO (0.88 μmol, TON_{CO} = 35.3) and HCOOH (0.97 μmol, TON_{HCOOH} = 39.0), and a high selectivity was observed for CO_2 reduction (92%) in the photocathodic compartment, while O_2 (1.02 μmol) was formed in the photoanodic compartment. Although a smaller photocurrent density was observed in this system, the faradaic efficiency of O_2 evolution significantly improved to F_{anode} = 98% with $F_{cathode}$ = 96%. The energy conversion efficiency equaled 2.0 × 10^{-2}% (Table 5). The selectivity of O_2 evolution in the system with the RhO_x/TaON photoanode was higher than that in the system with the $CoO_x/BiVO_4$ photoanode, which produced O_2 as well as H_2O_2, in line with previous reports.[58–60]

The mechanism of the photocatalytic reduction of CO_2 with water as the reductant in the full-cell system is illustrated in Scheme 5. Visible light is sequentially absorbed by the Ru(II) photosensitizer unit in the photocathode and n-type semiconductor ($BiVO_4$ or TaON) in the photocathode, in which a two-photon process, the so-called Z-scheme, induces electron transfer from the photoanode to the photocathode, and causes both strong reduction and oxidation powers on each side. The produced active electron is finally transferred to the Ru(II)

catalyst unit, and the hole is transferred to the co-catalyst (CoO_x or RhO_x).

These Z-scheme electron transfer processes continuously proceed during irradiation, inducing the two-electron reduction of one CO_2 molecule on the photocathode and the four-electron oxidation of two water molecules to furnish CO, HCOOH, and O_2 (partial two-electron oxidation of one water molecule to afford H_2O_2 also occurs on the $CoO_x/BiVO_4$ photoanode).

Conclusions

The introduction of a polypyrrole assembly into a dye-sensitized molecular photocathode as a connector between the redox photosensitizer, catalyst, and NiO electrode increased the photocatalytic performance of this electrode for CO_2 reduction, especially IPCE, which was more than three times higher than that of a previously reported dye-sensitized molecular photocathode constructed by the polymerization of vinyl groups instead of pyrrole groups. The maximum photocurrent was obtained even at a low applied potential ($E = -0.2$ V *vs.* Ag/AgCl). The durability of the modified photoelectrode was reasonably good, *i.e.*, 81% of the initial photocurrent was maintained even after 24 h irradiation. Full cells comprising this novel dye-sensitized molecular photocathode and the $CoO_x/BiVO_4$ or RhO_x/TaON photocathode could efficiently and selectively reduce CO_2 with water using visible light as the only energy source without any external bias, and the highest energy conversion efficiency was achieved in the reported full-cell systems with dye-sensitized molecular photocathodes.

Experimental

General procedures

^{1}H NMR (400 MHz) and ^{31}P NMR (162 MHz) spectra were recorded on a JEOL ECA400-II spectrometer. Transmission FT-IR spectra of metal complexes in MeCN were recorded using a JASCO FT/IR-6600 spectrometer at a resolution of 1 cm^{-1}. FT-IR spectra in DR mode were recorded using an FT/IR-6600 spectrometer equipped with a DR unit (DR-81, JASCO) at a resolution of 2 cm^{-1}. Electrospray ionization-mass spectroscopy (ESI-MS) analyses were performed using a Shimadzu LC-MS-2010 system with MeCN as the mobile phase. Inductively coupled plasma mass spectrometry (ICP-MS) analyses were performed in H_2O : HCl : H_2SO_4 (1 : 1 : 1) mixed acid solutions containing Ru complexes desorbed from the electrode. SEM images were obtained using a Hitachi S4700 system. The electrochemical analysis of metal complexes in MeCN solution and oxidative polymerization were performed in a three-electrode system using a BAS760Es electrochemical analyser. TOF-SIMS analyses were performed using a 5-100-AD instrument (ION-TOF GmbH). UV-vis absorption spectra in DR mode were recorded using a JASCO V-565 spectrophotometer. X-ray photoelectron spectra were recorded using a Shimadzu ESCA-4000 instrument, and Ru 3d and Cl 2p binding energies were corrected using the C 1s peak at 285.0 eV as a reference. The light responses of *I–V* curves during photoelectrochemical CO_2 reduction were measured using a Hokuto Denko potentiostat (Hokuto Denko HZ-7000) with a MAX 303 light source equipped with HOYA Y48 (λ > 460 nm) or L42 (λ > 400 nm) cutoff filters. Gas analysis was carried out using a micro-GC instrument (Agilent), and isotopic labelling studies were performed using GC-MS (Shimadzu MS-2010).

Materials

Acetonitrile (MeCN) was distilled twice after refluxing over P_2O_5 overnight and then distilled over CaH_2 immediately before use. Tetrabutylammonium tetrafluoroborate (Et_4NBF_4) was recrystallized from MeCN/ethyl acetate and then dried under reduced pressure at 373 K overnight before utilization. $^{13}CO_2$ (99% ^{13}C) was purchased from Cambridge Isotope Laboratories, Inc. $NaH^{13}CO_3$ (98% ^{13}C) was purchased from Sigma Aldrich. 4,4′-Bis(bromomethyl)-2,2′-bipyridine,[61] 1,2-bis(4′-methyl-[2,2′-bipyridin]-4-yl)ethane (bpyC_2bpy),[62] 4,4′-bis-(methylphosphonate)-2,2′-bipyridine ($(Et_2O_3PCH_2)_2$bpy),[61] $[Ru(dmb)_2]Cl_2$,[63,64] and $[Ru(CO)_2Cl_2]_n$[65] as well as NiO[10] and $CoO_x/BiVO_4$ (ref. 12) photoanodes were prepared as reported elsewhere. Pyrrole (TCI, >99%) was freshly distilled under reduced pressure and immediately used for synthesis. All other reagents and solvents were commercially available and used without further purification. The synthetic scheme and ^{1}H NMR spectra of all other metal complexes are given in the ESI† (SI-1).

Synthesis

4,4′-Bis((1*H*-pyrrol-1-yl)methyl)-2,2′-bipyridine (*Pyr*dmb). KOH pellets (1 g, 17.9 mmol) were crushed to a fine powder and transferred to a three-neck round-bottom flask kept under Ar flow. Dry dimethylformamide (DMF) (10 mL) was then injected into the flask, and the mixture was stirred. Freshly distilled pyrrole (1 mL, 15.42 mmol) was injected, and the mixture was left for 15 min until the solution turned pale yellow. 4,4′-Bis(-bromomethyl)-2,2′-bipyridine (0.5 g, 1.47 mmol) dissolved in DMF (5 mL) was dropwise added to the pale-yellow pyrrole–KOH mixture, and the solution was stirred at 25 °C overnight under Ar. The crude yellowish product was collected by precipitation in water and further extracted with dichloromethane (DCM) (3 × 50 mL) and the combined organic layers were evaporated to dryness. The crude product was purified by recrystallization from DCM–hexane to yield the final product as pale-yellow crystals (315 mg, 60.8%). ^{1}H NMR (400 MHz, $CDCl_3$) δ/ppm: 8.56 (d, $J = 4$ Hz, 2H), 8.21 (s, 2H), 6.88 (d, $J = 4$ Hz, 2H), 6.71 (t, $J = 2$ Hz, 4H), 6.23 (t, $J = 2$ Hz, 4H, C–H (Pyr)), 5.15 (s, 4H, –CH_2–). ESI-MS (in MeCN): m/z 315.0 $[M]^+$

[Ru(*Pyr*dmb)$_2$Cl$_2$]. A DMF solution of LiCl (56.73 mg, 1.34 mmol), $RuCl_3 \cdot xH_2O$ (50 mg, 0.191 mmol), and *Pyr*dmb (60.06 mg, 0.191 mmol) was refluxed under Ar for 2.5 h and extracted using DCM (4 × 30 mL). The combined organic layer was washed with water (4 × 15 mL), dried over anhydrous Na_2SO_4, and evaporated to dryness. The residue was purified by re-precipitation in DCM-diethyl ether to yield the final product as purplish black solids (76.4 mg, 81.2%). ^{1}H NMR (400 MHz, $CDCl_3$) δ/ppm: 10.05 (d, $J = 8$ Hz, 2H), 7.42 (dd, $J = 12$, 4 Hz, 8H), 6.73 (t, $J = 2$ Hz, 4H), 6.54 (t, $J = 2$ Hz, 4H), 6.45 (d, $J = 5.2$ Hz,

2H) 6.27 (t, $J = 2$ Hz, 4H), 6.18 (t, $J = 2$ Hz, 4H), 5.22 (s, 4H), 5.01 (s, 4H). ESI-MS (in MeCN): $m/z = 806.0$ $[M–Cl + MeCN]^+$.

[Ru(dmb)(*Pyr*dmb)Cl$_2$]. A solution of $[Ru(p\text{-cymene})Cl_2]_2$ (162.0 mg, 0.296 mmol) and 4,4′-dimethyl-2,2′-bipyridine (103 mg, 0.561 mmol) in MeCN (20 mL) was refluxed for 5 h under Ar and evaporated to afford [Ru(dmb)(*p*-cymene)Cl]Cl. ESI-MS (in MeCN) $m/z = 455$ $[M–Cl]^+$. [Ru(dmb)(*p*-cymene)Cl]Cl was then dissolved in MeCN (500 mL), and N_2 was bubbled into the solution for 30 min. The solution was then irradiated with a high-pressure Hg lamp (300 W) for 24 h, and the formation of $[Ru(dmb)(MeCN)_3Cl]Cl$ was confirmed by ESI-MS ($m/z = 444.0$ $[M–Cl]^+$). The black solid obtained after solvent removal was mixed with 4,4′-bis((1*H*-pyrrol-1-yl)methyl)-2,2′-bipyridine (*Pyr*dmb) (176 mg, 0.56 mmol) in 150 mL of an acetone–MeOH (5 vol%) mixture, and the solution was refluxed under Ar overnight. $[Ru(dmb)(Pyrdmb)Cl_2]$ was obtained by re-precipitation in DCM-diethyl ether as a purplish black solid. ESI-MS (in MeCN): $m/z = 670.0$ $[M]^+$.

[Ru(dmb)$_2$(*Pyr*dmb)](PF$_6$)$_2$ (PyrRu). A solution of $[Ru(dmb)_2Cl_2]$ (35.0 mg, 0.0647 mmol) and 4,4′-bis((1*H*-pyrrol-1-yl)methyl)-2,2′-bipyridine (25.0 mg, 0.0795 mmol) in ethanol (20 mL) was refluxed under Ar overnight and then evaporated. The crude product was extracted using 150 mL of a DCM–water (1 : 2) mixture containing 0.1 M NH_4PF_6, and the product was isolated from the organic layer. The crude solids were recrystallized from acetone–diethyl ether to yield the final product as red crystals (50 mg, 72%). ^{1}H NMR (400 MHz, acetone-d_6) δ/ppm: 8.39 (s, 4H), 7.98 (s, 2H), 7.66 (d, $J = 5.8$ Hz, 2H), 7.55 (dd, 5.8, 2 Hz, 4H); 7.29 (m, 4H); 7.01 (m, 2H), 6.85 (t, $J = 2.4$ Hz, 4H), 6.28 (t, $J = 2.4$ Hz, 4H), 5.36 (s, 4H), 2.57 (d, $J = 6$ Hz, 12H). ESI-MS (in MeCN): $m/z = 392.0$ $[M–2PF_6^-]^{2+}$. Elemental analysis: C (49.22%), H (3.81%), and N (10.25%), calculated for $C_{44}H_{42}N_8P_2F_{12}Ru$: C (49.15%), H (3.94%), and N (10.42%).

[Ru(*Pyr*dmb)$_2$(dmb)](PF$_6$)$_2$ (Pyr2Ru). A solution of $[Ru(Pyrdmb)_2Cl_2]$ (25.0 mg, 0.0313 mmol) and 4,4′-dimethyl-2,2′-bipyridine (8.0 mg, 0.0434 mmol) in ethanol (15 mL) was refluxed under Ar overnight and then evaporated. The crude product was extracted with 150 mL of a DCM–water (1 : 2) mixture containing 0.1 M NH_4PF_6. The product was isolated from the organic layer, and the obtained solids were precipitated from DCM–diethyl ether to yield the final product as red solids (19.8 mg, 51.2%). ^{1}H NMR (400 MHz, acetone-d_6) δ/ppm: 8.59 (s, 2H), 8.30 (s, 4H); 7.85 (dd, $J = 10.4$, 5.6 Hz, 4H), 7.70 (d, $J = 6$ Hz, 2H), 7.31 (d, $J = 5.6$ Hz, 2H), 7.0 (dd, 4H), 6.76 (dt, $J = 9.2$, 2 Hz, 8H), 6.11 (dt, $J = 9.2$, 2 Hz, 8H), 5.37 (d, $J = 4.4$ Hz, 8H), 2.49 (s, 6H). ESI-MS (in MeCN): $m/z = 457.0$ $([M–2PF_6]^{2+})$. Elemental analysis: C (51.86%), H (4.24%), and N (11.54%), calculated for $C_{52}H_{48}N_{10}P_2F_{12}Ru$: C (51.82%), H (4.02%), and N (11.61%).

[Ru(dmb)(*Pyr*dmb)((H$_2$O$_3$PCH$_2$)$_2$bpy)](PF$_6$)$_2$ (PRuPyr). A solution of $[Ru(dmb)(Pyrdmb)Cl_2]$ (30.0 mg, 0.044 mmol) and 4,4′-bis-(methylphosphonate)-2,2′-bipyridine ($(Et_2O_3PCH_2)_2bpy$) (51 mg, 0.112 mmol) in ethanol (20 mL) was refluxed overnight and evaporated. The residue was dissolved in water (15 mL), the solid was filtered off, and the solution was further washed with chloroform (3 × 5 mL). Saturated aqueous NH_4PF_6 (10 mL) and DCM (75 mL) were added, and the mixture was stirred for 2 h. The DCM layer was washed with water (3 × 10 mL) and dried over anhydrous Na_2SO_4. The solid obtained after evaporation was recrystallized from DCM and diethyl ether to yield the final product as red crystals (45.61 mg, 77%). $[Ru(dmb)(Pyrdmb)((Et_2O_3PCH_2)_2bpy)](PF_6)_2$ (40.0 mg, 0.037 mmol) was refluxed with bromotrimethylsilane (0.1 mL, 0.53 mmol) in MeCN (15 mL) under Ar overnight. The reaction mixture was cooled to room temperature and then evaporated. The obtained solid was dissolved in water (10 mL), and saturated aqueous NH_4PF_6 (5 mL) was added to precipitate $[Ru(dmb)(Pyrdmb)((H_2O_3PCH_2)_2bpy)](PF_6)_2$ (PRu*Pyr*) as a red solid, which was collected by filtration and sequentially washed with water and diethyl ether (24.0 mg, 67%). ^{1}H NMR (400 MHz, acetone-d_6) δ/ppm: 8.66 (s, 2H); 8.63 (s, 2H), 8.33 (s, 2H), 7.89 (m, 4H), 7.74 (m, 2H); 7.47 (m, 2H); 7.34 (d, $J = 6$ Hz, 2H), 6.97 (m, 2H), 6.75 (t, $J = 2$ Hz, 4H), 6.15 (t, $J = 2$ Hz, 4H), 5.39 (d, $J = 4.2$ Hz, 4H); 3.99 (m, 8H), 3.48 (d, $J = 4$ Hz, 2H), 3.43 (d, $J = 4$ Hz, 2H), 2.53 (s, 3H), 2.50 (s, 3H), 1.1 (m, 12H). ^{31}P NMR (162 MHz, acetone-d_6) δ/ppm: 23.11 (s, 2P, $-PO_3Et_2$), −144 (sep., 2P, PF_6^-). ESI-MS (in MeCN): $m/z = 528$ $([M–2PF_6]^{2+})$. Elemental analysis: C (44.98%), H (3.87%), N (9.08%), calculated for $C_{44}H_{44}N_8O_6P_4F_{12}Ru$: C (42.83%), H (3.59%), and N (9.08%).

[Ru(dmb)(*Pyr*dmb)(bpyC$_2$bpy)](PF$_6$)$_2$ (PyrRuC$_2$bpy). A solution of $[Ru(dmb)(Pyrdmb)Cl_2]$ (60 mg, 0.0895 mmol) and $bpyC_2bpy$ (98.5 mg, 0.269 mmol) in ethanol (20 mL) was refluxed overnight under Ar and then evaporated. The solid was taken up in water, the filtrate was washed with chloroform (3 × 10 mL) and supplemented with saturated aqueous NH_4PF_6 (5 mL). The product was extracted with DCM (3 × 50 mL), and the combined organic layer was dried over anhydrous Na_2SO_4 and evaporated to give a red precipitate. *Pyr*RuC_2bpy was separated by column chromatography on SP Sephadex C-25 (MeCN–H_2O 1 : 1, v/v) and recrystallized from acetone–ether to yield the final product as red solids (85.4 mg, 76%). ^{1}H NMR (400 MHz, acetone-d_6) δ/ppm, 8.76 (s, 2H), 8.61 (s, 4H), 8.52–8.42 (m, 2H), 8.30 (s, 2H), 7.93–7.73 (m, 6H), 7.50–7.40 (m, 2H), 7.37–7.28 (m, 2H), 7.26–7.16 (m, 2H), 7.04–6.94 (m, 2H), 6.75 (t, $J = 2.4$ Hz, 4H), 6.12 (t, $J = 2.4$ Hz, 4H); 5.38 (d, $J = 2.4$ Hz, 4H), 3.2 (m, 4H), 2.5 (m, 12H). ESI-MS (in MeCN): $m/z = 483$ $([M–2PF_6]^{2+})$. Elemental analysis: C (53.86%), H (4.09%), and N (11.39%), calculated for $C_{56}H_{52}N_{10}P_2F_{12}Ru$: C (53.86%), H (4.36%), and N (11.02%).

[Ru(dmb)(*Pyr*dmb)(bpyC$_2$bpy)Ru(CO)$_2$Cl$_2$](PF$_6$)$_2$ (PyrRuC$_2$RuCAT). A solution of $[Ru(dmb)(Pyrdmb)(bpyC_2bpy)](PF_6)_2$ (30 mg, 0.0239 mmol) and $[Ru(CO)_2Cl_2]_n$ (9 mg, 0.036 mmol) in EtOH–acetone (1 : 1, 10 mL) was refluxed for 5 h under Ar and then evaporated. The obtained red solid was recrystallized from acetone–ether to yield the final product as red solids (34 mg, 96%). ^{1}H NMR (400 MHz, acetone-d_6) δ/ppm: 8.98–8.88 (m, 2H); 8.37–8.17 (m, 6H), 7.85 (s, 2H), 7.60–7.35 (m, 8H), 7.22–7.02 (m, 4H), 6.94–6.86 (m, 2H), 6.73 (t, $J = 2.4$ Hz, 4H), 6.16 (t, $J = 2.4$ Hz, 4H), 5.24 (d, $J = 6.4$ Hz, 4H), 3.25 (d, $J = 7.8$ Hz, 4H), 2.5 (m, 12H). ESI-MS (in MeCN): $m/z = 597$ $([M–2PF_6]^{2+})$. FT-IR (cast film) ν_{CO}/cm^{-1}: 1996, 2060. Elemental analysis: C (47.26%), H (3.28%), N (9.58%); calculated for $C_{58}H_{52}N_{10}Cl_2O_2P_2F_{12}Ru_2$: C (47.27%), H (3.70%), and N (9.34%).

Fabrication of photocathodes

NiO/PRuPyr. The NiO electrode (area = 2.5 cm^2) was immersed into a MeCN–methanol (9 : 1, v/v) solution (4 mL) of PRu*Pyr* (5 μM) in the dark overnight, washed with MeCN–methanol (9 : 1, v/v), and dried in air. The total amount of the metal complex adsorbed on the NiO electrode (n_{PRuPyr}) was determined from the difference in the absorbance of the solution before and after adsorption as well as by the ICP-MS analysis of H_2O : HCl : H_2SO_4 (1 : 1 : 1) mixed acid solutions containing the Ru complex desorbed from the NiO/PRu*Pyr* electrode, as described later in detail.

Oxidative electropolymerization of the metal complexes on NiO and NiO/PRuPyr electrodes. A MeCN solution (8 mL) containing *Pyr*Ru, *Pyr*2Ru, *Pyr*RuC_2bpy, or *Pyr*RuC_2RuCAT (0.5 mM) and Et_4NBF_4 (0.1 M) as the supporting electrolyte was introduced into a one-component electrochemical cell. The NiO or NiO/PRu*Pyr* electrode, a Ag/$AgNO_3$ electrode (Ag wire immersed in MeCN containing 0.01 M $AgNO_3$ and 0.1 M Et_4NBF_4 separated by Vycor® glass), and a Pt wire were used as working, reference, and counter electrodes, respectively. After Ar gas was flown into the cell for 15 min, the potential was cycled between 0 and +1.35 V at 100 mV s^{-1}. The obtained electrodes were washed with MeCN and stored in air in the dark.

Introduction of Ru catalyst unit to electropolymerized electrodes. The electropolymerized electrode was soaked in a MeCN solution (4 mL) containing $[Ru(CO)_2Cl_2]_n$ (0.5 mM) for 24 h, washed with MeCN, and air-dried in the dark.

Estimation of the Ru complexes adsorbed on the electrodes and TONs. The amounts of electrochemically active Ru centers (n_{CV}/mol) were determined by cycling the electrodes between 0.4 and +1.2 V *vs.* Ag/$AgNO_3$ in MeCN solutions containing 0.1 M Et_4NBF_4 as a supporting electrolyte at 10 mV s^{-1},[12] and by using the following equation.

$$n_{CV} = S/Fv \quad (1)$$

where S is the area under the Ru(II)/(III) peak (A V), F is the Faraday constant (96 485 C mol^{-1}), and v is the scan rate (0.01 V s^{-1}). The areal density of electroactive Ru units was calculated by dividing n_{CV} by the area of the electrode (2.5 cm^2).

The total number of Ru units (n_{total}), that is, Ru photosensitizer units + RuCAT units adsorbed on the electrodes, was estimated by ICP-MS analysis of H_2O : HCl : H_2SO_4 (1 : 1 : 1) mixed acid solutions containing the Ru complexes desorbed from the electrodes. Similarly the total number of the photosensitizers estimated using the electrode after the step-2 (n_{PS}). The corresponding concentration was estimated from calibration plots prepared using the standard Ru atomic absorption standard solution (Aldrich, 1000 μg mL^{-1} Ru in 5% HCl). The amount of RuCAT units (n_{cat}) was estimated using eqn (2) and calculated as the average of four experimental trials, as shown in Tables S1–S4.†

$$n_{cat} = (n_{total} - n_{PS}) \quad (2)$$

Product TONs were calculated as

$$TON = [product]/n_{cat} \quad (3)$$

where [product] is the amount of the product, that is, CO, HCOOH, or H_2.

Fabrication of the RhO_x/TaON photoanode

Particulate TaON was prepared according to a previously reported method.[66] Ta_2O_5 (2 g) particles were heated in a flow of NH_3 (20 mL min^{-1}) at 1123 K for 15 h. Rh species (0.7 wt% metal basis) was loaded on TaON particles by impregnation with aqueous $Na_3[RhCl_6]\cdot nH_2O$ followed by heating at 673 K for 30 min in air to afford RhO_x/TaON.[55] The as-prepared RhO_x/TaON particles were deposited on a Ti substrate as follows. The particles (60 mg) were dispersed in acetone (25 mL) by 5 min sonication, and an aliquot of this dispersion (60 μL) was dropped onto the Ti substrate and dried in air at room temperature. The drop-casting/drying cycle was repeated 20 times. The representative amount of RhO_x/TaON particles on Ti was approximately 2.9 mg. The coated area was 1.5 cm × 4 cm. Post-necking was applied to provide sufficient conductivity between the particles as well as between the particles and the substrate.[55,57,66–69] The RhO_x/TaON electrodes were coated with 50 μL of methanolic $TaCl_5$ (10 mM) and then dried in air at room temperature. After this process was performed five times, the electrode was heated in an NH_3 flow (10 mL min^{-1}) at 723 K for 30 min.

Photoelectrochemical measurements and photocatalytic CO_2 reduction using dye-sensitized molecular photocathodes

The IPCEs of the electrodes were measured according to previous reports.[12,27] Photocatalytic performance was also evaluated using a previously reported method, with the vital parts briefly outlined below. Photoelectrochemical CO_2 reduction was conducted in a Pyrex H-shaped cell with two compartments containing aqueous $NaHCO_3$ (15–18 mL, 50 mM) and separated by a Nafion® film (Aldrich, Nafion 117). The working electrode (photocathode) and a Ag/AgCl reference electrode were placed in the cathode compartment, while a Pt wire counter electrode was placed in the anode compartment. The three-electrode setup was connected to a potentiostat (HZ-7000, Hokuto Denko). The reaction was conducted by flowing CO_2 into the cathode compartment for 30 min. The photoanode was irradiated using a 300 W Xe lamp (MAX-303, Asahi Spectra) equipped with a cutoff filter (HOYA Y48 for λ_{ex} = 460–650 nm) and the CO and H_2 produced in the gas phase were analyzed using a micro-GC MGC3000A (Inficon), while HCOOH in the solution was analyzed using a capillary electrophoresis apparatus (Agilent 7100 L, Otsuka Electronics).

Photocatalytic CO_2 reduction with water oxidation (two-compartment setup)

The reaction was carried out using the two-compartment cell and setup explained in the previous section, except that a CoO_x/$BiVO_4$ or a RhO_x/TaON photoanode was used instead of a Pt wire counter electrode. An HZ-7000 potentiostat was used in the non-resistance ammeter mode. The photocathode (2.5 cm^2) was

irradiated at λ_{ex} = 460–650 nm using a 300 W Xe lamp with a cutoff filter. $CoO_x/BiVO_4$ (1.2–2.0 cm^2) was irradiated at λ_{ex} = 400–650 nm using a 300 W Xe lamp (Asahi Spectra, MAX-302) with a cutoff filter (HOYA, L42) and an IR-cut filter. CO, H_2, HCOOH, and O_2 were analyzed as described previously for half-cell experiments.

ECE (%) was calculated as

$$\mathrm{ECE} = E_{\mathrm{chemical}}/E_{\mathrm{photon}} \times 100\% \quad (4)$$

where E_{photon} is the total energy of irradiated photons calculated as P_1 (32.0 mW cm^{-2} × 2.5 cm^2) + P_2 (28.0 mW cm^{-2} × 1.55 cm^2) × irradiation time (18 000 s) = 2.22 kJ. The total chemical energies of the generated CO, HCOOH, and H_2 ($E_{chemical}$) were calculated using eqn (5)–(8).

$$CO_2 \rightarrow CO + 0.5O_2\ \Delta G^0 = +257\ \mathrm{kJ\ mol^{-1}}: \Delta E^0 = 1.33 \quad (5)$$

$$CO_2 + H_2O \rightarrow HCOOH + 0.5O_2\ \Delta G^0 = +270\ \mathrm{kJ\ mol^{-1}}: \Delta E^0 = 1.43\ \mathrm{V} \quad (6)$$

$$H_2O \rightarrow H_2 + 0.5O_2\ \Delta G^0 = +237\ \mathrm{kJ\ mol^{-1}}: \Delta E^0 = 1.23\ \mathrm{V} \quad (7)$$

$$E_{\mathrm{chemical}} = \Sigma[\mathrm{product}] \times 2FV_{\mathrm{theoretical}} \quad (8)$$

where [product] is the amount of generated CO, HCOOH, and H_2, F is the Faraday constant, $V_{theoretical}$ is the theoretical formation voltage for each product, and E_{photon} is given by the integration of irradiated light energy.

Photocatalytic CO_2 reduction with water oxidation (one-compartment setup)

In a tandem cell with a one-compartment setup, the photocathode and photoanode were placed in a face-to-face configuration. The HAL-320 (Asahi Spectra, light intensity = 100 mW cm^{-2}) lamp containing a built-in AM 1.5G filter (350–1100 nm) was used as a single light source for irradiation. The photocathode was irradiated from the back side, and the photons transmitted through this electrode then reached the front side of the photoanode.

Data availability

All the data supporting this article have been included in the main text and the ESI.†

Author contributions

Fazalurahman Kuttassery: most of experiments and writing of manuscript. H. Kumagai: photoanode preparation and discussion. Ryutaro Kamata: methodology and discussion. Yusuke Ebato: setting up of gas analysis system, discussion, Masanobu Higashi: photoanode preparation, Hajime Suzuki: photoanode preparation, Ryu Abe: photoanode preparation and discussion, Osamu Ishitani: conceptualization, funding acquisition, and supervision; writing, review, and editing of manuscript.

Conflicts of interest

There are no conflicts to declare.

Acknowledgements

This work was supported by JST CREST grant number JPMJCR13L1 in "Molecular Technology," JST Strategic International Collaborative Research Program (PhotoCAT), and JSPS KAKENHI Grant numbers JP20H00396 and JP17H06440 in Scientific Research on Innovative Areas "Innovations for Light-Energy Conversion (I4LEC)". We thank Center for Advanced Materials Analysis, Tokyo Institute of Technology for the SEM, ICP-MS and TOF-SIMS measurements.

Notes and references

1 M. Z. Jacobson, *Energy Environ. Sci.*, 2009, **2**, 148–173.
2 S. C. Peter, *ACS Energy Lett.*, 2018, **3**, 1557–1561.
3 H. Takeda and O. Ishitani, *Coord. Chem. Rev.*, 2010, **254**, 346–354.
4 Y. Yamazaki, H. Takeda and O. Ishitani, *J. Photochem. Photobiol., C*, 2015, **25**, 106–137.
5 Y. Tamaki, T. Morimoto, K. Koike and O. Ishitani, *Proc. Natl. Acad. Sci. U.S.A.*, 2012, **109**, 15673–15678.
6 Y. Tamaki and O. Ishitani, *ACS Catal.*, 2017, **7**, 3394–3409.
7 Y. Tamaki, K. Watanabe, K. Koike, H. Inoue, T. Morimoto and O. Ishitani, *Faraday Discuss.*, 2012, **155**, 115–127.
8 K. Maeda, *Adv. Mater.*, 2019, **31**, 1808205.
9 G. Sahara, R. Abe, M. Higashi, T. Morikawa, K. Maeda, Y. Ueda and O. Ishitani, *Chem. Commun.*, 2015, **51**, 10722–10725.
10 G. Sahara, H. Kumagai, K. Maeda, N. Kaeffer, V. Artero, M. Higashi, R. Abe and O. Ishitani, *J. Am. Chem. Soc.*, 2016, **138**, 14152–14158.
11 H. Kumagai, G. Sahara, K. Maeda, M. Higashi, R. Abe and O. Ishitani, *Chem. Sci.*, 2017, **8**, 4242–4249.
12 R. Kamata, H. Kumagai, Y. Yamazaki, M. Higashi, R. Abe and O. Ishitani, *J. Mater. Chem. A*, 2021, **9**, 1517–1529.
13 K. Sekizawa, S. Sato, T. Arai and T. Morikawa, *ACS Catal.*, 2018, **8**, 1405–1416.
14 S. Sato, T. Arai, T. Morikawa, K. Uemura, T. M. Suzuki, H. Tanaka and T. Kajino, *J. Am. Chem. Soc.*, 2011, **133**, 15240–15243.
15 Q. Wang, J. Warnan, S. Rodríguez-Jiménez, J. J. Leung, S. Kalathil, V. Andrei, K. Domen and E. Reisner, *Nat. Energy*, 2020, **5**, 703–710.
16 C. D. Windle and R. N. Perutz, *Coord. Chem. Rev.*, 2012, **256**, 2562–2570.
17 Y. Kou, S. Nakatani, G. Sunagawa, Y. Tachikawa, D. Masui, T. Shimada, S. Takagi, D. A. Tryk, Y. Nabetani, H. Tachibana and H. Inoue, *J. Catal.*, 2014, **310**, 57–66.
18 B. H. Farnum, K.-R. Wee and T. J. Meyer, *Nat. Chem.*, 2016, **8**, 845–852.
19 T.-T. Li, B. Shan and T. J. Meyer, *ACS Energy Lett.*, 2019, **4**, 629–636.
20 B. Zhang and L. Sun, *Chem. Soc. Rev.*, 2019, **48**, 2216–2264.

21 P. D. Tran, V. Artero and M. Fontecave, *Energy Environ. Sci.*, 2010, **3**, 727–747.
22 R. L. House, N. Y. M. Iha, R. L. Coppo, L. Alibabaei, B. D. Sherman, P. Kang, M. K. Brennaman, P. G. Hoertz and T. J. Meyer, *J. Photochem. Photobiol., C*, 2015, **25**, 32–45.
23 F. Li, H. Yang, W. Li and L. Sun, *Joule*, 2018, **2**, 36–60.
24 D. Wang, Q. Huang, W. Shi, W. You and T. J. Meyer, *Trends Chem.*, 2021, **3**, 59–71.
25 A. K. Vannucci, L. Alibabaei, M. D. Losego, J. J. Concepcion, B. Kalanyan, G. N. Parsons and T. J. Meyer, *Proc. Natl. Acad. Sci. U.S.A.*, 2013, **110**, 20918–20922.
26 D. Wang, F. Niu, M. J. Mortelliti, M. V. Sheridan, B. D. Sherman, Y. Zhu, J. R. McBride, J. L. Dempsey, S. Shen and C. J. Dares, *Proc. Natl. Acad. Sci. U.S.A.*, 2020, **117**, 12564–12571.
27 R. Kamata, H. Kumagai, Y. Yamazaki, G. Sahara and O. Ishitani, *ACS Appl. Mater. Interfaces*, 2019, **11**, 5632–5641.
28 J. Mola, E. Mas-Marza, X. Sala, I. Romero, M. Rodríguez, C. Viñas, T. Parella and A. Llobet, *Angew. Chem., Int. Ed.*, 2008, **47**, 5830–5832.
29 L. Wang, K. Fan, H. Chen, Q. Daniel, B. Philippe, H. Rensmo and L. Sun, *Catal. Today*, 2017, **290**, 73–77.
30 D. L. Ashford, A. M. Lapides, A. K. Vannucci, K. Hanson, D. A. Torelli, D. P. Harrison, J. L. Templeton and T. J. Meyer, *J. Am. Chem. Soc.*, 2014, **136**, 6578–6581.
31 D. L. Ashford, B. D. Sherman, R. A. Binstead, J. L. Templeton and T. J. Meyer, *Angew. Chem., Int. Ed.*, 2015, **54**, 4778–4781.
32 L. Wu, A. Nayak, J. Shao and T. J. Meyer, *Proc. Natl. Acad. Sci. U.S.A.*, 2019, **116**, 11153–11158.
33 A. Deronzier and J. C. Moutet, *Acc. Chem. Res.*, 1989, **22**, 249–255.
34 D. Martineau, M. Beley, P. C. Gros, S. Cazzanti, S. Caramori and C. A. Bignozzi, *Inorg. Chem.*, 2007, **46**, 2272–2277.
35 L. Wang, K. Fan, Q. Daniel, L. Duan, F. Li, B. Philippe, H. Rensmo, H. Chen, J. Sun and L. Sun, *Chem. Commun.*, 2015, **51**, 7883–7886.
36 A. Deronzier and J.-C. Moutet, *Coord. Chem. Rev.*, 1996, **147**, 339–371.
37 S. Cosnier, A. Deronzier and J.-C. Moutet, *J. Electroanal. Chem. Interfacial Electrochem.*, 1986, **207**, 315–321.
38 S. Cosnier, A. Deronzier and J.-C. Moutet, *J. Mol. Catal.*, 1988, **45**, 381–391.
39 J. Ochmanska and P. G. Pickup, *J. Electroanal. Chem. Interfacial Electrochem.*, 1989, **271**, 83–105.
40 G. I. Dzhardimalieva, L. N. Rabinskiy, K. A. Kydralieva and I. E. Uflyand, *RSC Adv.*, 2019, **9**, 37009–37051.
41 A. Riul, D. S. dos Santos, K. Wohnrath, R. Di Tommazo, A. C. P. L. F. Carvalho, F. J. Fonseca, O. N. Oliveira, D. M. Taylor and L. H. C. Mattoso, *Langmuir*, 2002, **18**, 239–245.
42 A. Deronzier, P. Jardon, A. Martre, J.-C. Moutet, C. Santato, V. Balzani, A. Credi, F. Paolucci and S. Roffia, *New J. Chem.*, 1998, **22**, 33–37.
43 T. Arai, S. Sato, K. Uemura, T. Morikawa, T. Kajino and T. Motohiro, *Chem. Commun.*, 2010, **46**, 6944–6946.
44 T. Arai, S. Sato, T. Kajino and T. Morikawa, *Energy Environ. Sci.*, 2013, **6**, 1274–1282.
45 S. Sato, T. Arai and T. Morikawa, *Inorg. Chem.*, 2015, **54**, 5105–5113.
46 T. Arai, S. Sato and T. Morikawa, *Energy Environ. Sci.*, 2015, **8**, 1998–2002.
47 Y. Tamaki, K. Tokuda, Y. Yamazaki, D. Saito, Y. Ueda and O. Ishitani, *Front. Chem.*, 2019, **7**, 327.
48 J.-M. Lehn and R. Ziessel, *J. Organomet. Chem.*, 1990, **382**, 157–173.
49 S. Chardon-Noblat, A. Deronzier, R. Ziessel and D. Zsoldos, *Inorg. Chem.*, 1997, **36**, 5384–5389.
50 G. Balducci, E. Iengo, N. Demitri and E. Alessio, *Eur. J. Inorg. Chem.*, 2015, **26**, 4296.
51 Y. Kuramochi, J. Itabashi, K. Fukaya, A. Enomoto, M. Yoshida and H. Ishida, *Chem. Sci.*, 2015, **6**, 3063–3074.
52 C. W. Machan, M. D. Sampson and C. P. Kubiak, *J. Am. Chem. Soc.*, 2015, **137**, 8564–8571.
53 A. Iwase, H. Ito, Q. Jia and A. Kudo, *Chem. Lett.*, 2016, **45**, 152–154.
54 A. Iwase, S. Ikeda and A. Kudo, *Chem. Lett.*, 2017, **46**, 651–654.
55 M. Higashi, Y. Kato, Y. Iwase, O. Tomita and R. Abe, *J. Photochem. Photobiol., A*, 2021, **419**, 113463.
56 R. Abe, M. Higashi and K. Domen, *J. Am. Chem. Soc.*, 2010, **132**, 11828–11829.
57 M. Higashi, K. Domen and R. Abe, *J. Am. Chem. Soc.*, 2012, **134**, 6968–6971.
58 K. Fuku and K. Sayama, *Chem. Commun.*, 2016, **52**, 5406–5409.
59 K. Fuku, Y. Miyase, Y. Miseki, T. Funaki, T. Gunji and K. Sayama, *Chem.–Asian J.*, 2017, **12**, 1111–1119.
60 K. Sayama, *ACS Energy Lett.*, 2018, **3**, 1093–1101.
61 G. Will, G. Boschloo, S. N. Rao and D. Fitzmaurice, *J. Phys. Chem. B*, 1999, **103**, 8067–8079.
62 L. Sun, H. Berglund, R. Davydov, T. Norrby, L. Hammarström, P. Korall, A. Börje, C. Philouze, K. Berg, A. Tran, M. Andersson, G. Stenhagen, J. Mårtensson, M. Almgren, S. Styring and B. Åkermark, *J. Am. Chem. Soc.*, 1997, **119**, 6996–7004.
63 G. Gaines Jr, P. Behnken and S. Valenty, *J. Am. Chem. Soc.*, 1978, **100**, 6549–6559.
64 W. Wacholtz, R. Auerbach and R. Schmehl, *Inorg. Chem.*, 1987, **26**, 2989–2994.
65 P. A. Anderson, G. B. Deacon, K. H. Haarmann, F. R. Keene, T. J. Meyer, D. A. Reitsma, B. W. Skelton, G. F. Strouse and N. C. Thomas, *Inorg. Chem.*, 1995, **34**, 6145–6157.
66 G. Hitoki, T. Takata, J. N. Kondo, M. Hara, H. Kobayashi and K. Domen, *Chem. Commun.*, 2002, 1698–1699.
67 M. Higashi, K. Domen and R. Abe, *Energy Environ. Sci.*, 2011, **4**, 4138–4147.
68 M. Higashi, K. Domen and R. Abe, *J. Am. Chem. Soc.*, 2013, **135**, 10238–10241.
69 M. Higashi, O. Tomita and R. Abe, *Top. Catal.*, 2016, **59**, 740–749.